32nd Student Research Day & Industry Open House

Abstract Volume

April 28th 2017

Department of Earth and Atmospheric Science,
University of Houston
Houston, Texas 77204

EDITORS

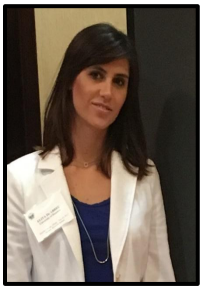

Elita De Abreu received her Bachelor's (2006) and Master's degree (2010) in Physics from Universidade Estadual de Campinas - UICAMP. In 2006 she joined the Exploration team in Petrobras where she performed quantitative seismic interpretation and rock physics simulation in the Campos, Santos and Sergipe-Alagoas basins. She is a former SEG Wavelets president, UH Energy Ambassador and chair of EAS Grad Committee. She is currently a Vice-Chair of Internal Affairs of Energy Coalition and is pursuing her PhD in The Effects Of Bandwidth Extension On Seismic Amplitude And Phase with Dr. Castagna at University of Houston.

Committee Chair - Kirstie L. Haynie received two B.S. degrees, with honors, in Geophysics and Mathematics at the University of Houston in 2014. After completing an undergraduate thesis in the field of remote sensing, Kirstie dived directly into the Ph.D. program at UH where she pursued Geodynamics with advisor Dr. M. A. Jadamec. Apart from teaching Physical Geology and being involved with the Badminton Club of UH, which she co-founded, Kirstie spends most of her time running and analyzing results from high-resolution 3D numerical models of the Alaska subduction zone in an attempt to understand the effects of oceanic plateau subduction-collision.

Faculty advisor for Student Research Day – Dr. Regina Capuano is an Associate Professor of Geosciences at the University of Houston. She completed her PhD in Geology at the University of Arizona in 1988.

INDEX

Oral Presentations

INTEGRATED BASIN AND PLAY ASSESSMENT OF UNDISCOVERED OIL AND GAS RESOURCES IN THE WESTERN CARIBBEAN SEA: MISKITO BASIN, COLOMBIAN OFFSHORE

CARVAJAL, L. C.

Known hydrocarbon occurrences are indicative of a widespread and active, offshore petroleum system in the western Caribbean Sea where exploration campaigns since the 50s have recovered hydrocarbons ranging from 21° to 45° API. In this study, the combination of both exploration results and geological characteristics were combined in order to estimate locations for petroleum occurrence within a realistic illustration of spatial distribution of undiscovered petroleum potential, under different confidence levels for exploration decision-making. The data integrated into the play analysis included ~13,000 km of 2D seismic data, 32 wells with geological and drilling information, petrophysical data, and geochemical data including total organic content (TOC%), kerogen types, transformation ratio, hydrogen index, oxygen index and paleoheat flows. The superimposed mapping of geological factors that control hydrocarbon accumulation, integrated with isopachs, lithofacies, seismic facies, structural features and paleogeography models, were used to evaluate the Miskito basin. Miskito area was assessed as low-, medium-, and high- exploration risk, with high and low confidence levels based on data coverage. Thus, Miskito basin defined is defined with high confidence level based on good well density and seismic coverage, fewer oil and gas shows, low TOC % with high oxygen index, good reservoir facies including deltaic sands and isolated carbonates reefs with uneven seal distribution. This study illustrates the strength of regional geology in the western Caribbean region and its impact on proper risk analysis in a favorability map as a useful tool for future exploration campaigns.

LATITUDINAL VARIATION IN SALT-BODY INTERVAL VELOCITIES IN THE DEEPWATER GULF OF MEXICO: KEATHLEY CANYON AND WALKER RIDGE AREAS

CORNELIUS, S. AND J. P. CASTAGNA

Borehole measurements of salt-body compressional-wave interval velocities from 55 wells in the vicinity of the Keathley Canyon and Walker Ridge areas of the Gulf of Mexico vary from 13,966 ft/s (4256 m/s) to 18,535 ft/s (5649 m/s) with mean velocity of 14,920 ft/s (4547 m/s) and a standard deviation of 726 ft/s (221 m/s). The velocities vary significantly with latitude. Five different interval velocity zones have been identified with each having specific associated mineralogies within a latitude range. In the mid-latitude zones, sylvite, various clastics, and small traces of both anhydrite and gypsum, are found within the salt, yielding salt-body interval velocity variation from 14,388 ft/s to 14,965 ft/s (4386 m/s to 4544 m/s). The salt interval velocity in the southern limits of the study area is higher than 15,000 ft/s (4572 m/s) and associated with more gypsum. The northern most wells are anhydrite-rich and exhibit the highest velocities. The interval velocities are relatively uncorrelated to and insensitive to factors such as wellbore temperature, depth, and pressure. Composite medium modeling of the salt-body compositions shows that compositional variation within the salt body can explain the observed velocity variations.

THE EFFECT OF PROPPANT-FILLED FRACTURES ON THE ELASTIC PROPERTIES OF 3D-PRINTED ROCK MODELS

DANDE, S., R. R. STEWART, N. DYAUR, AND J. BAZE-FRANCESCHI

The role of the proppant in hydraulic fracturing is to keep open or "prop" the induced fractures. However, not all fractures propped. Determining the distribution of propped fractures is important to understand further the flow of hydrocarbons and microseismic event locations. In this study, our goal is to investigate whether any variations in the velocities of propped materials could be diagnostic of fracture fill by proppant. To undertake experiments on a known physical model, we use 3D-printing technology. We printed two models (with orthorhombic symmetry – horizontal layering and vertical cracks), one with open and originally air-filled fractures (hereafter called A model) and another with proppant-filled fractures (hereafter called the P model) and used them in our laboratory study. The density and porosity of model A are 0.763 g/cc and 24% respectively. After filling fractures with proppant, the density of model P increased to 0.822 g/cc and porosity decreased to 21%. We observed approximately 10% reduction in both P and S velocities from model A to model P. We observed 40% increase in P-wave velocity when model A saturated with water and proppant. Shear velocity further decreased by 10% when proppant added to the water saturated model. We also estimated the dimensionless orthorhombic Thomsen style P-wave anisotropic coefficients for two models to characterize the likely anisotropic behavior of the material. While we observed a negligible change in ε1, a significant change in P-wave anisotropy ε2 is observed from +0.012 (A) to -0.041 (P). Negative ε indicates a decrease in P-wave velocity when P-wave propagates perpendicular to proppant-filled fractures. The magnitude of S-wave splitting at vertical incidence decreased by 6% from dry model A to model P. This study shows strong evidence of a difference in elastic wave velocities and anisotropy varying with proppant. This may prove very useful for hydraulic fracture monitoring and stimulated and propped reservoir volumes.

THE USE OF DEEP LEARNING TO PREDICT OZONE CONCENTRATION OVER HOUSTON AREA

ESLAMI, E. AND Y. CHOI

The potential use of deep belief network for forecasting hourly ozone concentration over Houston-Galveston-Brazoria area (HGB) are discussed using deep belief network. Air quality forecasting is a recognized analytical challenge which been primarily carried out by physical models. In this study, a new approach by using deep belief network has been proposed to overcome this data intensive forecasting challenge. The deep learning approach used air quality-related variables as predictors throughout the spatial domain of (HGB) to make a prediction for hourly ozone concentration in September 2013. Meteorological parameters such as wind field, temperature, relative humidity, and cloud fraction along with the ozone and NOx concentrations were used as input predictors. Continuous Ambient Monitoring Station (CAMS) operated by Texas Commission on Environmental Quality (TCEQ) was used to acquire observation data of both meteorology and air pollution. North American Regional Reanalysis (NARR) was used for cloud fraction. Two supervised deep learning approaches, stacked MLP and sparse feature learning, were used for the ozone forecasting system. The proposed deep models analyze different input data by identifying the higher level features abstracted from lower level features of these data using a stepwise manner. These automatically learned features are appropriate for quantifying the relationship between different parameters. Identifying such relationship will help to achieve more accurate ozone matter forecasting system in metropolitan areas.

EFFECTS OF VARIATIONS IN FLUID PROPERTIES AND FRACTURE GEOMETRY ON DISPERSION, ANISOTROPY AND REFLECTION IN MEDIA WITH PLANAR FRACTURES

GAN, Y. AND E. CHESNOKOV

Our objective was to discover the effect of variations in fluid properties and fracture geometry on the velocity of seismic wave propagation in fluid-saturated media with parallel planar fractures. We used numerical models to examine the behavior of P-wave phase velocity dispersion in the normal direction to layering, in non-porous and porous media with planar fractures. We also examined the anisotropy of low frequency phase and group velocities of fast and slow P-waves and angular dependent reflection coefficients in media with planar fractures, under conditions of saturation by fluids with varying bulk moduli, densities, and fracture apertures. We defined several parameters in order to characterize dispersion, anisotropy, the difference between fast and slow modes, and reflection. Our results show that these parameters have different sensitivities to contrast variation of properties among solids and fluids, apertures and fracture spacing when saturated by various fluids; for some cases, the range can also be different. Our results are helpful in distinguishing fluid types saturating geophysical fractures and estimating the aperture and spacing of planar fractures. In seismic exploration, bulk modulus and fluid density can provide useful information in distinguishing among brine, oil, and gas; fracture geometry is important to estimate the permeability of reservoirs.

TECTONIC DRIVERS OF THE WRANGELL BLOCK: INSIGHTS ON FOREARC SLIVER PROCESSES FROM 3D GEODYNAMIC MODELS OF ALASKA

HAYNIE, K. L. AND M. A. JADAMEC

Intracontinental shear zones can play a key role in understanding how plate convergence is manifested in the upper plate in regions of oblique subduction. However, the relative role of the driving forces from the subducting plate and the resisting force from within intracontinental shear zones is not well understood. Results from high-resolution, geographically referenced, instantaneous 3D geodynamic models of flat slab subduction at the oblique convergent margin of Alaska are presented. These models investigate how viscosity and length of the Denali fault intracontinental shear zone as well as coupling along the plate boundary interface modulate motion of the Wrangell block forearc sliver and slip across the Denali fault. The 3D models predict along strike variation in offset along the Denali fault, changing from dextral strike-slip motion in the eastern segment to oblique convergence towards the fault apex. Models further show that the flat slab drives oblique motion of the Wrangell block and contributes to 20% (models with a short fault) and 28% (models with a long fault) of the observed Quaternary slip rates along the Denali fault. In addition, models with a weak Denali fault (10^{17} Pa s) and strong plate coupling (10^{21} Pa s) were found to produce the fastest motions of the Wrangell block (~ 10 mm/yr). The 3D models provide insight into the general processes of forearc sliver mechanics and also offer a 3D framework for interpreting hazards in regions of flat slab subduction.

APPLICATION OF THE DIRECT WAVEFORM INVERSION ON 2D MODELS

lIU, Z. AND Y. ZHENG

The Direct Waveform Inversion (DWI) is a new full-waveform inversion idea that is different from current full waveform inversion (FWI) procedures. DWI combines the seismic imaging and velocity inversion into one process. The DWI uses the full seismic wavefield including multiples and recursively invert for the velocity model in a shallow-to-deep fashion by explicitly using the time-space causality. Therefore, we do not need a global initial velocity model and the absolute convergence is reached when the deep reflections are beyond the finite recording time. DWI offers new possibilities to overcome the challenges in many model perturbation based inversion methods, whose effectiveness largely depends on the quality of initial model and nonlinear optimization schemes. We present numerical applications of DWI on two models: a layered model and a 2D model. DWI can successfully invert for both models using full wavefield data where reflections and multiples are present in data.

SPECTRAL DECOMPOSITION USING TIME-FREQUENCY CONTINUOUS WAVELET TRANSFORMS FOR FAULT DETECTION IN THE BAKKEN FORMATION

JAHAN, I. AND J. CASTAGNA

Spectral decomposition was applied using time-frequency continuous wavelet transforms to a Bakken Formation 3D seismic dataset. Principal component analysis was used to detect discontinuities on different iso-frequency volumes. Faults with different vertical displacement were preferentially highlighted at different dominant frequencies. At the Bakken level, major faults showed best at low frequencies, while antithetic faulting around the master faults showed best at high frequencies.

WEST TEXAS MICRO EARTHQUAKES INDUCED OR NOT

JING, H. AND H. W. ZHOU

Micro-earthquakes occurred in Permian basin West Texas, are mainly associated with petroleum production related activities, such as oil & gas extraction and wastewater disposal injection. With available passive seismic data from EarthScope USArray projects, we determined and located 126 micro-earthquakes within the area of -100° W ~ -104.5° W, 30.5° N ~ 33.5° N, from 03/2009 to 02/2010. Two major earthquakes in this area trembled on 03/10/2010 and 03/11/2010; their focal mechanism analysis shows they occurred along an active fault plane. Wastewater disposal injection volume data supports these two major events are induced.

STABLE AND RADIOGENIC Mg ISOTOPE STUDY OF THREE SIMILAR EARLY SOLAR SYSTEM REFRACTORY SOLIDS: CAIs

KEREKGYARTO, A., R. JEFFCOAT, AND M. RIGHTER

Ca-Al-rich inclusions (CAIs) are some of the earliest formed crystalline solids in our developing solar nebula. Their mechanisms and timing of formation provide clues about the conditions in and development of the early solar system. The short-lived radionuclide 26Al, which decays to 26Mg (t1/2 = .705 My, β+), is a major early heat source and useful as a high-precision chronometer for early solar system solids. Since 26Al is an extinct radionuclide, only relative ages can be established via resolving the initial radioactive 26Al present during formation, commonly discussed as (26Al/27Al)0. This is done by correlating excess radiogenic 26Mg of phases with their 27Al/24Mg values to show an isochronous relationship. Using 'bulk rock' (in this case, bulk CAI) measurements or fragments representing the whole for isotope studies are appropriate when the system in question remains closed throughout its history. If any mineral-scale isotopic resetting or even complete isotopic homogenization subsequent to formation, bulk measurements would average everything and still represent the initial formation. Evidence of open system conditions has been increasingly seen in CAIs, implying that bulk measurements of these objects would not reflect the timing and conditions of initial formation. Using more conventional means of mineral separation and wet chemistry reduce/remove spatial resolution and homogenize sub-mineral isotopic variations. We prefer in situ methods (LA-MC-ICPMS) correlated with detailed petrographic evidence to resolve these sub-mineral and mineral scale isotopic variations. We present in situ stable and radiogenic Mg isotopic work from three CAIs which share many rare petrographic features in effort to correlate early, time-significant events from multiple internal isochrons.

CHARACTERIZATION OF WIND PATTERNS OVER TEXAS: IMPACT ON DALLAS-FORT WORTH OZONE

KOTSAKIS, A., Y. CHOI, A. SOURI, AND J. FLYNN

Over the last 15 years, Dallas-Fort Worth (DFW) has seen a decrease is ozone exceedances similar to the trends seen for the Houston area. Both of these decreasing trends are largely due to the implementation of stricter regulations on ozone precursors primarily nitrogen oxides (NOx). While the decrease in ozone exceedances due to decreased ozone precursors is relatively well understood, the variability in meteorology and its impact on ozone trends in DFW is not. To gain a better understanding of the meteorological patterns that have historically lead to ozone exceedances over the DFW area, a wind pattern analysis was done. Wind patterns were identified and classified for different ozone regimes over the Dallas-Fort Worth. The frequency of each pattern was analyzed to determine if certain patterns to become more or less frequent over time and if this has also impacted ozone trends. Finally, the potential relationship between Houston pollution transport to DFW was examined.

ISOTROPIC-FRACTURED FLUID-SATURATED LAYER: DISPERSIVE PROPERTIES AND TUNING EFFECTS

KRYLOVA, A.

We make use of the averaging of the elastic properties of the fluid-filled fractured rock for different laws of the random fracture distribution with consideration of propagation of the extremely slow and dispersive Krauklis wave within individual fractures. The presence of the Krauklis wave contributes to an increase of P-wave velocity dispersion and attenuation with the decrease of frequency. The comparison of the P-wave reflection coefficients for various acoustic impedance distributions expose remarkable difference of the frequency and angular dependency for fractured and homogeneous layers. The results exhibit the thickness related tuning effects deviation of the fractured layer from non-fractured.

GEOCHEMICAL MODELS FOR TWO COMPONENTS MIXING FROM ARCTIC MORB

LING, X., J. SNOW, AND Y. LI

The presence of enriched components in the mid-ocean ridge (MOR) mantle is widely discussed. The variety of the components is commonly correlated with nearness to hotspots, residual mantle composition and ridge depth. The ultra-slow spreading Gakkel Ridge and Lena Trough are known to be the best locations to investigate mantle heterogeneity with a low melt productivity. The potassium enriched MORB (K-MORB) composition from Central Lena Trough (CLT) specifies a heterogeneous mantle source with possible garnet existing under low pressure. This study is to explore the basaltic mantle sources beneath the area by carrying out multiple models and calculating melting P-T conditions. Here the melting models and thermodynamic calculations quantified the possible mantle sources composition, the degree of melting and the melting condition for CLT basalt. We conclude that the CLT basalt bulk composition is the mixture of N-MORB-like North Lena Trough (NLT) basalt and a H2O-K rich melt from low degree melting of depleted mantle, phlogopite and pargasitic amphibole. Therefore the binary mixing of the two exists in the studying region. This kind of result infers to the tectonic evolution of the area during the Arctic Ocean opening.

A POTENTIAL IMPACT SITE IN THE SAHARA DESERT, REMOTE SENSING EVIDENCE AGAINST FORMATION FROM ANAOROGENIC MAGMATISM OF THE AÏR MOUNTAINS, NIGER

LOBPRIES, T.

Satellite images reveal a previously unreported, roughly 10 km in diameter, circular feature in north-central Niger, Africa. The circular feature is located within Paleozoic marine sedimentary strata of Early to Middle Devonian age and is about 100 km to the north of a world-class suite of ring dikes located in the Aïr Mountains. These dikes appear similar in structure to a bolide (meteoritic) impact and occur within a large Paleoproterozoic granitic massif. Remote sensing of this inaccessible site provides initial reconnaissance that could lead to ground truth investigation and provides implications for applying similar techniques in other isolated regions as well as in planetary remote sensing studies. Evidence based on remote sensing analyses of Landsat 8 data indicates that the Niger structure did not form as a magmatic intrusion close to the time of deposition and posits that it formed from either a bolide impact at least 40-60 million years after deposition or by some other geologic process, but the results are somewhat inconclusive. Techniques using the ENVI software platform, band ratios/math from Landsat 8, and Spaceborne Imaging Radar-C were used to determine the composition and structure of the potential impact site host rock and compare this to the ring plutons of the Aïr Mountains and sedimentary rock outcrops in the region. In order to quantify the ambiguous results, spectral profile plots were created for each endmember rock type and compared to the Niger site. These spectral profile plots reveal the basis for the inconclusive analyses with variations existing for each endmember making comparison and classification difficult. Recently released satellite datasets for Sentinel 2 were then used to produce similar spectral profile plots at a higher resolution of 10-20m per pixel (depending on the band) versus the 30m resolution of Landsat8. These plots reveal greater distinction between endmembers and allow for their classification. So, classification of Sentinel 2 datasets allows for more accurate identification of outcrop and land cover types and indicates that the Niger site is sedimentary, not plutonic, making it more likely to be an impact feature.

SIMULTANEOUS DETERMINATION OF ORGANOSULFUR COMPOUNDS, DIAMONOIDS, AROMATIC AND SATURATED BIOMARKERS IN CRUDE OILS BY GAS CHROMATOGRAPHY-TRIPLE QUADUPOLE MASS SPECTROMETRY

MEI, M., K. K. A. BISSADA, T. B. MALLOY, L. M.DARNELL, AND E. B. SZYMCYK

An improved GC-MS/MS method with expanded multiple reaction monitoring (MRM) transitions in specific time windows was developed for simultaneous determination of various types of molecular markers including organosulfur compounds (OSC), diamondoids, saturated and aromatic biomarkers in whole crude oils to eliminate the need for laborious group-type separation steps and separate analyses of the various fractions. The method was tested using four crude oils of diverse types and maturities: a heavy crude from the Mediterranean, an intermediate-density crude from the Arabian Gulf, a light black oil from California, and a light condensate from Wyoming (API 18°, 33°, 39°, and 53°, respectively). The optimization was achieved through improving GC separation and increasing selectivity and sensitivity in MRM settings (selective choice of precursor and product ions, specified collision energies, dwell time, and time windows). Under optimum conditions, the improved method was validated by checking accuracy and precision using three spiking levels of standard compounds into the oils. Comparison of the improved GC-MS/MS method for simultaneous determination of diverse geochemical-marker groups in whole-crudes with the traditional approaches that entail rigorous separation of group-types and subsequent assorted GC-MS analysis protocols, indicates that the whole-oil GC-MS/MS analysis approach achieved higher resolution, higher specificity and sensitivity, higher accuracy and comparable precision for calculation of the common biomarker indices. This improved approach efficiently eliminates the requirement of prior chromatographic separation, avoids the loss of light-end components during sample preparation, alleviates the need for multiple analyses for different groups of compounds and minimizes co-elution problems in biomarker analyses.

COMPARISON OF ANISOTROPIC EFFECTIVE MEDIUM SCHEMES FOR ELASTIC INTERACTIONS OF INCLUSIONS

MORSHED, S. M. AND E. M. CHESNOKOV

Understanding of effective elastic properties of the reservoir rock is essential for meaningful interpretation and analysis of seismic measurements. However, most of the effective medium theories fail to account elastic interactions of inclusions at high crack density. Therefore, an investigation on the role of elastic interaction of the inclusions in the effective medium schemes has been done. We study the effective elastic properties of multiphase media containing low to high concentrations of isolated pores. Randomly oriented spherical pores and horizontally oriented ellipsoidal (aspect ratio =0.1) pores have been considered. Three different methods such as Generalized Singular Approximation (GSA), Grain contact (GC) and Sevostianov & Giraud's (SG) method have been examined. Both GSA and SG allow inclusions beyond dilute concentrations of ellipsoidal cracks. For isolated spherical pores, all the three methods show exactly same or similar results. However, inclusion interactions are different in different directions in case of horizontal ellipsoidal pores and individual stiffness constants differ greatly from one method to another at different concentrations of crack density. Stiffness constants remain consistent and stable in GSA method whereas some components become unusual in SG method at a higher crack density (>0.15).

EVALUATION OF THE AIR QUALITY IMPACTS OF INCREASED FREIGHT TRAFFIC IN THE HOUSTON METROPOLITAN AREA IN A FUTURE YEAR

PAN, S., Y. CHOI, AND A. ROY

The Houston Metropolitan region is the 4th largest urban area nationally and classified as a nonattainment area for ozone by the U.S. Environmental Protection Agency. Additionally, it is in borderline attainment for fine particulate matter (PM2.5). Transportation sources in urban areas, predominantly from vehicular traffic (gasoline motor vehicles and diesel trucks), are the major sources of nitrogen oxides (NOx) and Volatile Organic Compounds (VOCs), which can react in the presence of sunlight to form ozone. In addition to ozone precursors, vehicular traffic also emits important components of particulate matter such as organic and elemental carbon. As indicated by the 2013 H-GAC Regional Goods Movement Plan, the population of the Houston Area is projected to grow by 50% in 2040, which could potentially result in an increased trucking and other freight activity to meet the needs of the growing population. It is therefore imperative to carry out an impact analysis study going into the future, which could evaluate the air quality impacts of the increased transportation activity, the effects of control technologies and strategies. In this study, we developed future projections for trucking emissions, and evaluated various emissions scenarios related to electric vehicles and varying levels of emission control. These emissions scenarios include: (1) a current-year case; (2) a “business as usual” case, where the trucking fleet in 2040 will have the same emission factors as in 2011; (3) an “intermediate emissions” case, where reasonable fractions for fleet turnover are assumed; (4) a “Best Case” where all trucks in 2040 are fitted with the control technologies resulting in a highest reduction in emissions; (5) an “All Electric Transportation” case, where trucks in the region are all converted to electricity. Each emissions scenario was used in a fine resolution (1 km) chemical transport model to estimate its impacts on regional PM2.5 and ozone. Results indicated that ozone concentrations (with ~2 ppb change) had different changing features between urban and outflow regions. PM2.5 concentrations (with ~1 ug/m3 change) generally followed the change of emissions.

SEDIMENT CHARACTERIZATION OF TILLS AND GLACIOMARINE DIAMICTONS IN THE ROSS SEA, ANTARCTICA: SUBSTRATE DEFORMATION AND ICE SHEET BEHAVIOR

ROBINSON, D.

Antarctica contains the largest ice mass on earth, comprised of complex ice sheets that have been advancing and retreating since the onset of glaciation in the late Eocene or earliest Oligocene. The Ross embayment is the outlet for one-third of all Antarctic ice flow, receiving input from both East and West Antarctica, which contributes to global sea-level changes. Marine-based ice streams expand and contract across the Ross Sea continental shelf, eroding the substrate and transporting sediment subglacially. The sediment underlying the ice experiences significant deformational strain from ice mass movement, altering the physical characteristics of the sediment and leaving records of glacial cyclicity. This study uses sediment characteristics, representing compression loading and unloading of the sediments by an ice sheet, to differentiate major episodes of ice sheet advance and retreat in the Ross Sea. The lateral extent of the maximum grounding line for the Last Glacial Maximum (26.5-19 ka) is not clearly constrained by direct geologic evidence. Fabric analyses and characterization of sand grain shape and texture will allow the detailed understanding needed to differentiate diamictons of different depositional processes, and therefore provide a tool for determining the position of the paleo-grounding line of the ice sheet. The depositional strain levels recorded in the modern sediments will establish a classification scheme applicable to older, more ambiguous Ross Sea sediments. Ultimately, better tools for discriminating between subglacial and proximal glaciomarine deposits will allow for more detailed reconstructions of ice-sheet history, and thus determine the forcing mechanisms to which the ice is responding.

GEOCHEMISTRY OF THE RIO GRANDE RIFT MANTLE LITHOSPHERE

SCHAFFER, L., A. PESLIER, AND A. BRANDON

Major and trace element concentrations of peridotite xenoliths were measured at two locals along the Rio Grande Rift, (NM, USA); Kilbourne Hole and Rio Puerco. These two locales are idea to test the hypothesis that the southern Rio Grande Rift is underlain by shallow asthenosphere that was emplaced during Farallon slab rollback. Southern locale Kilbourne Hole can be geochemically divided into two groups based on trace element element geochemistry. One group has depleted light rare earth element (LREE) signatures associated with melting processes, while the second group has enriched LREE signatures associated with metasomatic events. The northern locale, Rio Puerco, contains peridotites that are enriched in LREE, indicating that these samples have undergone more extensive metasomatism. Binary mixing models between potential metasomatic fluids and melt residues indicate that both regions were metasomatized by a combination of silicate and carbonatite fluids that are associated with the subduction of the Farallon slab. Based on the similar metasomatic signatures observed between the two locales, it is unlikely that lithosphere delamination occurred in the southern Rio Grande Rift, and that Kilbourne Hole xenoliths represent mantle lithosphere, not asthenosphere.

PALEOGENE TECTONICS DRAINAGE DYNAMICS AND BASIN FILLING IN NORTH CENTRAL NEW MEXICO

SMITH, T., K. SUNDELL, S. JOHNSTON, C. G. ANDRADE, R. ANDREA, J. DICKINSON, J. SAYLOR, Y. LIU, M. MURPHY, AND T. LAPEN

Paleogene Laramide basin development and sediment provenance are recorded in fluvial deposits of north-central New Mexico. Specifically, the El Rito, Galisteo and Diamond Tail formations are critical archives of Laramide deformation and associated drainage network dynamics. However, timing of El Rito Formation deposition is poorly understood due to a lack of biostratigraphic age control, which has led to a tenuous correlation with the Galisteo Formation. This correlation carries with it significant implications for sediment source and tectonic activity. We present newly measured stratigraphy and ancillary provenance information, together with detrital zircon U-Pb geochronology to elucidate the fluvial evolution and relationship among these formations. This research supports a south-flowing El Rito trunk fluvial system fed by eastward flowing tributaries proposed by previous authors. However, contrary to clast-counts, we identify unique detrital zircon signatures, supported by paleocurrents, that change in response to hinterland tectonic activity. These data suggest that Galisteo deposition was coeval with formation of the basal El Rito unconformity rather than the deposition of the El Rito Formation. Furthermore, El Rito stratigraphic architecture records waning Laramide tectonic activity in surrounding local uplifts.

REMOTE SENSING EVIDENCE OF DECADAL CHANGES IN MAJOR TROPOSPHERIC OZONE PRECURSORS OVER EAST ASIA

SOURI, A. H., Y. CHOI, W. JEON, J. H. WOO, Q. ZHANG, AND J. I. KUROKAWA

Recent regulatory policies in East Asia reduce ozone precursors, but these changes are spatially and temporally nonuniform. This study investigates variations in the long-term trends of tropospheric NO2, HCHO, and HCHO/NO2 ratios to diagnose ozone sensitivity to changes in NOx and volatile organic compound using the Ozone Monitoring Instrument (OMI). Using an adaptive-degree polynomial filter, we identify extremums of time series of NO2 to determine when and how NO2 change. Due to the regulations in China, trends which were predominantly upward turned downward. The years undergoing these changes primarily happened in 2011 and 2012. OMI column densities, however, suggest that NOx sources in South Korea, the Pearl River Delta (PRD), Taiwan, and Japan have not consistently decreased. Specifically, as Chinese exports of NO2 started subsiding, increasing trends in NO2 columns over several Korean cities, including Seoul, become evident. To quantify the changes in NOx emissions from summertime 2010 to 2014, we conduct a 3D-Var inverse modeling using a regional model with MIX-Asia inventory and estimate NOx emissions (in 2010 and 2014) for the PRD (1.6 and 1.5 Gg/d), the Yangtze River Delta (3.9 and 3.0 Gg/d), north China (15.6 and 14.3 Gg/d), South Korea (1.6 and 1.5 Gg/d), and Japan (2.7 and 2.6 Gg/d). OMI HCHO shows upward trends in East Asia resulting from anthropogenic effects; however, the magnitudes are negative in the PRD, Japan, North Korea, and Taiwan. OMI HCHO/NO2 ratios reveal that while South Korea, Japan, and the south of China have undergone toward more NOx-sensitive regime, areas around the Bohai Sea have become more NOx saturated.

GROUND BASED HYPERSPECTRAL IMAGING OF THE EAGLE FORD FORMATION

SUN, L. AND S. KHAN

This study used ground-based hyperspectral imaging to map an outcrop of the Eagle Ford Formation in west Texas. The Eagle Ford Formation consists of alternating layers of limestones, marlstones and volcanic ashes with high total organic content deposited during the Cenomanian-Turonian oceanic anoxic event. It is one of the few unconventional source rock and reservoirs that have surface representations. Hyperspectral remote sensing acquires electromagnetic radiation in numerous bands in a continuous spectrum and holds great potential to resolve mineralogical compositions without physical damage. Ground-based hyperspectral imaging scans the geologic outcrops at close ranges with very fine spatial resolution (millimeters to centimeters). Pixel-based spectral modeling identified absorption features from clay and calcite minerals, and fitted Gaussian functions to represent absorptions. Gaussian fitting allowed quantification of mineral abundances, and classification allowed quantification of area covered by each rock type. Laboratory spectroscopy and thin section petrography are used to assist with mineral identification and data interpretation. Detailed hyperspectral imaging of an outcrop of the Eagle Ford Formation shed light on the distribution of lithologies. These data helped in creating a virtual outcrop model with mineral compositions, and provided geologic analogs to extract compositional and geo-mechanical characteristics. The utilization of these new techniques in geo-statistical analysis provides a workflow for employing remote sensing in resource exploration and exploitation.

UNMIXING DETRITAL ZIRCON U-PB AGE DISTRIBUTIONS

SUNDELL, K. E. AND J. SAYLOR

Detrital zircon U-Pb geochronology has become an invaluable technique in addressing source-to-sink sediment provenance. Despite recent advances in quantitative methods of data comparison, there is currently no widely accepted method of unmixing detrital age distributions. We developed an inverse Monte Carlo mixture model that determines relative contributions of source samples by comparing randomly weighted source sample age distributions to mixed samples using the Kolmogorov-Smirnov (KS) test D statistic, Kuiper test V statistic, and Cross-correlation coefficient. We demonstrate the utility of this model through a series of tests on synthetic data and empirical data from modern river sediments and catchment sources in Colombia, and loess samples from central China. Proof-of-concept tests show the model is capable of reproducing relative proportions of highly complex age distributions when both source and target samples are fully characterized. Results from modern river sand and loess samples that cannot be perfectly matched provide a cautionary note by demonstrating inadequate characterization of either sediment sources or mixed samples; this highlights the importance of such characterization for accurate interpretation of sediment provenance. Although comparison methods used yield comparable results, the Cross-correlation coefficient outperforms the KS and Kuiper test D and V statistics by matching known sample contributions with lower residuals and fewer model trials. This method has been developed into a MATLAB-based stand-alone executable (.exe file) graphical user interface that is freely available to the scientific community.

TOPOGRAPHY-COUPLED RESONANCE BETWEEN MARS NORMAL-MODES AND PHOBOS TIDAL FORCE

TIAN, Y.

Phobos is the largest moon of Mars. The gravity attraction of Phobos to Mars is a periodic force, which may excite seismic waves inside Mars. Since Phobos is below the synchronous orbit, its orbit is continuously decreasing due to the tidal effect. This will result in a monotonic increase in its orbital frequency, which may eventually intrude into the seismic normal-mode frequency range to cause resonance. The objective of this research is to investigate whether such a resonance phenomenon can occur and what the consequence is. As we know, resonance happens when the periodic tidal force has a similar frequency as that of martian normal modes. The resonance may cause large amplitude of ground vibration of Mars. From our calculation, when the resonance happens, the energy dissipation rate will be greatly increased, which will make Phobos falling much faster. Eventually, Phobos will hit Mars in a very short time. Our research may give us a new prospective on early formation of planets.

TIMING OF CRUSTAL SUTURING IN THE PAMIR

VILLARREAL, D, P., J. CHAPMAN, I. OIMAHMADOV, B. MACDONALD, B. CARRAPA, M. GADOEV, AND A. ROBINSON

The Pamir Mountains form the western syntax of the Himalayan-Tibetan orogeny and are composed of three tectonic terranes: the Northern Pamir, the Central Pamir, and the Southern Pamir that are separated by the Tanymas suture and Rushan-Pshart suture, respectively. The Northern Pamir is part of the Paleozoic-Late Triassic southern margin of Asia and was once bounded to its south by the Paleotethys Ocean. The Central and Southern Pamir were part of Gondwana until the Carboniferous when they rifted as crustal fragments and drifted northward towards the Northern Pamir during the early Permian. One of the outstanding questions in the region is the timing of suturing between the Gondwana derived terranes and the southern margin of Asia. Geochronologic results and Late Triassic-Early Jurassic terrigenous deposits suggest that the timing of collision between the Northern Pamir and the Central Pamir, which created the Tanymas suture, was coeval with the collision between the Central and Southern Pamir, which formed the Rushan-Pshart suture, during the Late Triassic to Early Jurassic Cimmerian Orogeny. However, some studies have suggested that the timing of suturing was not coeval, but instead, the Tanymas suture formed during the Early Jurassic while the Rushan-Pshart suture formed during the Late Jurassic. Nevertheless, with either interpretation, the presence of a Jurassic carbonate directly overlying terrigenous deposits within the southern Pamir suggest that the Cimmerian Orogeny did not involve a significant amount of crustal thickening. Recent analyses show that the post-suturing late Triassic to early Jurassic terrigenous sandstone located within the Southern Pamir have a strong Late Triassic arc signature. This Late Triassic arc signature could only have been derived from the Karakul Mazar terrane of the Northern Pamir. The results suggest that; 1) collision between the southern margin of Asia and all Gondwanan terranes was completed by the Early Jurassic (Hettangian), and 2) the northern Pamir were topographically elevated relative to the Central and Southern Pamir upon closure of the Paleotethys Ocean.

LABORATORY MEASUREMENTS OF VELOCITY DISPERSION AND WAVE ATTENUATION IN WATER SATURATED SANDSTONES AT LOW FREQUENCY

WEI, Q., D. H. HAN, AND Q. HUANG

We have conducted the laboratory measurements of elastic parameters of dry and partially water-saturated sandstones at frequency range from 2Hz to 500 Hz. Two sandstone samples with similar porosity of 20% but different permeability of 33 and 1830 mD. The experiments were performed with the low frequency apparatus, utilizing the force deformation principle. The measured results indicate that degree of water-saturation, rock permeability and measured frequency have significant impact on elastic properties and attenuation of the sandstones. With vacuum dried condition, both samples show ignorable velocity dispersion and low wave attenuation. With increasing water saturation, bulk modulus of sandstone tends to remain a constant until near fully saturated condition (~1% gas saturation), then increase sharply. Data suggest that a minimum amount of gases cause low bulk modulus and negligible dispersion. With transition from partial gas saturation to fully water saturation status, there is a trend to drastically increase bulk modulus with dispersion from a low to a high value with a transition band in frequency ranged from 2 Hz to 500 Hz. In addition, wave attenuation data show consistent response in frequency domain. The dramatically increased attenuation associates time scales of fluid resonant between rock frame and pore-inlet tube. However, shear modulus data show different trends from bulk modulus one that there are no relations with status of pore fluid saturation.

A LAYER-CELL APPROACH OF NEAR-SURFACE FIRST-ARRIVAL TOMOGRAPHY

WO, Y. AND H. W. ZHOU

Near-surface variations in topography and low-velocity weathering zone reduce the quality of onshore reflection seismic data, and a common remedy is applying static corrections based on a good estimation of near-surface velocities from turning ray tomography. For areas of rapid variations in the topography and the thickness of the weathering zone, we propose to unite two tomographic model parameterizations, the cell tomography and deformable layer tomography (DLT), in estimating near-surface velocities. This layer-cell approach estimates long-wavelength velocity variations first using DLT, and then determines the short-wavelength velocity variations further using cell tomography. Tests with the synthetic and field datasets demonstrate that the layer-cell tomographic approach is able to achieve solution models better than that using one of the two model parameterizations alone. The stacked sections of the field data from a mountain area show clear improvement after static corrections using the velocity model from the layer-cell approach.

DELINEATING BEACH AND DUNE MORPHOLOGY FROM MASSIVE TERRESTRIAL LASER SCANNING DATA USING THE GENERIC MAPPING TOOLS

ZHOU, X., G. WANG, Y. BAO, L. XIONG, V. GUZMAN, AND T. KEARNS

Terrestrial laser scanning (TLS) techniques have been proven to be efficient tools to collect three-dimensional high-density and high-accuracy point clouds for coastal research and resource management. However, TLS collects a massive amount of surveying points. The processing and presenting of the large volumes of datasets is always a challenge for research when targeting a large area with high-resolution. This article introduces a practical workflow using shell-scripting techniques to chain together tools from the Generic Mapping Tools (GMT), Geographic Resources Analysis Support System (GRASS), and other command-based open-source utilities for automating TLS data processing. TLS point clouds acquired in the beach and dune area near Freeport, Texas in May 2015 were used for the case study. GMT is an open source collection of programs designed for manipulating and displaying geographic data sets. Shell scripts for rotating the coordinate system, removing anomalous points, assessing data quality, generating high-accuracy bare-earth digital elevation models (DEMs), and quantifying changes of beach and sand dune features (shoreline, cross-shore section, dune ridge, toe, and volume) are presented in this article. This investigation indicated that GMT provides efficient and robust programs for regridding and filtering massive TLS point cloud data sets, for generating and displaying high-resolution DEMs, and for finally producing publication-quality maps and graphs. The methods and scripts presented in this article will benefit a large research and application community of geomorphologists, geologists, geophysicists, engineers, and others who need to handle large volumes of topographic datasets and generate high-resolution DEMs.

Poster Session

UNDERGRADUATE STUDENTS

GRAVITY-BASED STUDY OF FLEXURE AND CRUSTAL STRUCTURE AT THE NIGER AND MISSISSIPPI DELTAS

AJALA, R.

Thick deltas deposited on passive margins provide natural laboratories for gravity modeling of isostatic compensation and crustal flexure of the underlying, thinned continental and oceanic crust. I use published seismic reflection data, refraction stations, well data, and sediment thickness maps as constraints to investigate the crustal structure beneath two of the world's thickest deltas: the Niger delta in southern Nigeria and the Mississippi delta located in the northern Gulf of Mexico. I apply process-oriented gravity modeling (POGM) to both margins to estimate the finite strength of their underlying lithospheres. Results from POGM suggest that the Mississippi delta sediment deposited on a lithosphere that is significantly stronger than the lithosphere beneath the Niger Delta. A lithosphere with an elastic thickness of 48 km best explains the observed gravity anomaly in the Mississippi delta region. However, an elastic thickness increment from 20 km to 33 km in the Niger delta region is estimated and suggests that the lithosphere beneath the Niger delta increased in strength following the formation of the margin after Cretaceous rifting. I have applied traditional methods of gravity modeling approach based on discrete blocks of varying densities to refine the crustal structure of both the Niger and Mississippi deltas. Using these elastic thickness constraints, I use 3D flexural models for both deltas to predict areas of concentric subsidence and uplift due to compensation and compare these predicted areas of uplift and subsidence to topographic and bathymetric maps of the delta areas.

STRATIGRAPHIC THICKNESS, TOTAL ORGANIC CARBON VALUES, AND SOURCE ROCK TYPES PRODUCED BY OCEANIC ANOXIC EVENTS ON ATLANTIC AND GULF OF MEXICO PASSIVE MARGINS

CARR, P.

Oceanic anoxic events (OAEs) are short-lived periods of global oceanic oxygen deficiency triggered by massive volcanic eruptions. Previous work has identified eight OAEs worldwide: 1) OAE1A Selli event of 124.2-123.4 Ma age produced by Aptian Ontong Java Plateau eruptions in the Pacific Ocean; 2) OAE1B consists of a series of sub-OAE events: Urbino event of 110.9-110.6 Ma age, Paquier event of 112-111.6 Ma age and the Jacob event of 113.6-113.2 Ma age, all produced by Albian Kerguelen Plateau eruptions in the Indian Ocean; 3) OAE 1C Tollebuc event of 103.7-103.4 Ma age was volproduced by Albian South America-Africa breakup; 4) OAE1D Breistroffer event of 100.6-100.2 Ma age produced by Albian South America-Africa breakup; 5) OAE2 Bonarelli event of 93.8-93.5 Ma age produced by Turonian Caribbean Plateau eruptions in the Caribbean Sea; and 6) OAE3 event of 87.3-84.6 Ma age produced by Coniacian-Santonian Caribbean Plateau eruptions. These eight periods of intense, volcanic eruptions are recorded stratigraphically by the conformable and global deposition on the world's passive margins of continuous intervals of dark gray to black, pyrite-rich shale with total organic carbon (TOC) contents ranging from 1 to 20%. Because these intervals are widespread and reach such high TOCs, they are considered some of the best and most prolific source rock intervals for hydrocarbon accumulations especially when inter-fingered with sandy, turbiditic reservoirs in deep-water, passive margin-type settings. I have compiled the extent and thickness of OAEs on Atlantic and Gulf of Mexico passive margins using published well data. This data shows that OAE1 can vary in thickness from 100-1500 m with a TOC values in the range of 1.9-20%. OAE2 thicknesses range from 50–490 m with TOC values in the range of 2-10%. OAE3 thickness up to 100 m with TOC values in the range of 4-5%.

VISUALIZING GLOBAL SUBDUCTION ZONES WITH 3D IMMERSIVE VIRTUAL REALITY

CHANG, B.

With the advancement of digital data in science visualizing three-dimensional geologic features through point cloud data allows for constructing a real-time interactive 3D examination of geoscience data. Here, we show a comparison of different slab morphologies from three major global data sets rendered through the open source software, ShowEarthModel, which runs on 3D immersive Virtual Reality platforms as well as on desktop. For example, each point in the cloud is representative of an earthquake in three-dimensional space thus conveying a surface representing the geometrically complex spatial variations within Wadati-Benioff zones. This provides a more accurate method of exploring three-dimensional features in the Earth by placing expected slabs within context of their regions and the examination of subducting plate geometries show the along strike variations in slab dip and depth. ShowEarthModel combines the point cloud data of global subduction zones with the topographic features above each plate providing the opportunity for real-time evaluation of hypotheses.

FAULT AND RIVER TERRACE DEVELOPMENT IN THE MADISON VALLEY: IMPLICATIONS FOR FAULT SYSTEM BEHAVIOR AND PASSAGE OF THE YELLOWSTONE HOTSPOT

CHENIN, J.B. AND J.M. CANNON

Although active extensional systems are widespread throughout the Yellowstone area (i.e. Jackson Hole, Paradise Valley, and the Ruby Valley) their geometries vary significantly which has led to two competing hypothesis explaining their development: 1) Extension is driven by thermal expansion during passage of the Yellowstone hotspot and, 2) Regional E-W extension associated with basin and range tectonics. To better understand the spatiotemporal relationship between extension and these two tectonic drivers, I have carried out preliminary field and satellite imagery mapping of the Madison Range extensional system integrated with dated locations of the Yellowstone hotspot and regional kinematic data from the Northern Basin and Range. My results show that although the most recent surface ruptures occurred along west-dipping normal faults, the patterns of alluvial fan development suggest that the master fault is east-dipping and strikes parallel to the Gravelly Range. Detailed mapping near the Palisades Campground along the Madison River reveals an east-dipping synthetic fault which offsets the 2.0 Ma Huckleberry Tuff by approximately 40 m. At this location, the Huckleberry Tuff consists of three units whose textures can be attributed to different cooling histories. The lower and upper unit are a fine grained-rhyolite, with the middle unit containing larger quartz phenocrysts exhibiting welding. Overall, all three units are compositionally similar. Structural analysis of second order fault planes and fractures of this fault indicates that it accommodates N60E - S60W extension. Holocene activity of this fault is assessed by mapping its relationship with terrace risers of the Madison River. Four terraces were mapped along with their intervening risers (T0 – T3) where only the oldest T3 terrace is offset by this fault. Previously published data on the age of the Madison River terraces is sparse however we can constrain the age of T0 being approximately 11.5 Ka, constraining potential fault activity since then. However, the presence of the Yellowstone hotspot since 0.65 Ma suggests a longer-lived system. This portion of the geologic history is likely obscured by Holocene glacial activity (120 – 20 Ka). Future work will integrate previously published maps of glacial moraines to interrogate the geologic history they record.

GROUND-BASED HYPERSPECTRAL DETECTION OF GOLD-BEARING HYDROTHERMAL ALTERATION ZONES AT THE GOLDSTRIKE MINING DISTRICT, UT

CROCKETT, M. AND S. D. KHAN

This study seeks to distinguish and map complex phases of hydrothermal alteration in the Goldstrike Mining District near St. George, Utah in order to understand the origin, genesis, and depositional controls on gold mineralization as well as quantifying and predicting the extent of the deposit. Goldstrike is a structurally complex region hosting disseminated gold deposits in permeable sedimentary layers near high angle fault zones. These fault zones, the original conduit for gold-bearing hydrothermal fluids, are highly silicified and often gold-bearing themselves, but alteration patterns are complex, difficult to distinguish visually, composed of several phases, and vary significantly over centimeter to meter scale distances. This makes identifying and quantifying the extent of the target zones costly, time consuming, and discontinuous with traditional geochemical methods. Ground-based hyperspectral scans in both SWIR and VNIR ranges have been taken of vertical exposures of both gold-bearing and barren silicified rocks (jasperoids) across several mine sites, with the intent to produce complete images delineating and quantifying the range of each phase of alteration. Due to the short distance to the outcrops, the scans enable continuous, high resolution spectroscopic analysis.

REGIONAL COMPARISON OF DETRITAL ZIRCONS POPULATIONS IN PRE-RIFT PALEOZOIC AND SYN-RIFT MESOZOIC ROCKS FROM THE GULF OF MEXICO TO NORTHERN SOUTH AMERICA AND NORTH AMERICA

KOUASSI, M.

In an effort to identify similar age populations linking tectonic blocks in the Gulf of Mexico to the Amazonian craton and evaluate existing plate reconstruction models for the pre-rift and syn-rift paleogeography, I have compiled 8,672 detrital zircon ages collected by various groups of previous workers of Paleozoic and Mesozoic ages and covering the area of rifting between southern North America, Mexico and northern South America. The dataset was first qualitatively analyzed through the inspection of stacked probability density plots displaying the main age populations and their respective proportions. Then using K-S Test D-values represented as multi-dimensional scaling (MDS) plots, quantitative comparison was performed. The detrital zircon age distributions of the Paleozoic strata from the Maya, Mixteca, Oaxaquia and Suwannee, initially similar to the coeval Colombian Eastern Cordillera strata as opposed to the Colorado Plateau strata, become less similar by the Mesozoic time. This initial strong affinity to the Colombian Eastern Cordillera implies that the terranes might have been derived from the same source. Thus, in a closed fit reconstruction all of these areas may have been overlain by a common basin that covered the present-day area of the GOM, Yucatan block, and northern South America. Similarly, increased dissimilarity of the target terranes data to the Colombian Eastern Cordillera and increased similarity to the Colorado Plateau in the Triassic-Jurassic time can be related to the formation and later fragmentation of Pangea which separated the peri-Gondwanan terranes from Gondwana and left them accreted to the southern margin of Laurentia.

HETEROGENEITY IN THE UNCOMPAHGRE UPLIFT REFLECTED IN PROXIMAL-DISTAL SEDIMENT MIXING IN THE PARADOX BASIN

LAMBERT, K. J., T. M. SMITH, J.E. SAYLOR, T.J. LAPEN, AND P. COPELAND

The Uncompahgre Uplift is one of several basement-cored uplifts thought to exhume primarily metamorphic rocks of the Yavapai (1.7-1.8 Ga) terrane during the evolution of the Ancestral Rocky Mountains (ARM). The timing of exhumation is primarily constrained by ages of synorogenic strata in the adjacent Paradox Basin. Previous detrital zircon U-Pb geochronology from Paradox Basin alluvial fans that are proximal to the Uncompahgre Uplift record a unimodal 1.4-1.5 Ga signature which was unidentified in the adjacent northern uplift. In contrast, fluvial deposits in the medial-distal Paradox Basin include a bimodal mixture of 1.4-1.5 Ga zircons along with 1.7-1.8 Ga zircons. While the 1.7-1.8 Ga signature is easily explained by exhumation of Yavapai terrane crust in the Uncompahgre Uplift, the origin of the 1.4-1.5 Ga zircons was unclear. We address the origin of these enigmatic 1.4-1.5 Ga zircons by conducting zircon U-Pb analyses of basement samples collected from an east-west traverse through Unaweep Canyon which transects the northern Uncompahgre Uplift. Analyses of the meta-igneous and meta-sedimentary basement rocks show a dominance of middle Proterozoic ages of 1.7 Ga equivalent to Yavapai terrane, with secondary contributions of 1.4-1.5 Ga ages, demonstrating that the northern Uncompahgre Uplift is actually comprised of 1.4-1.8 Ga rocks. We conclude that the unimodal detrital zircon signature from the proximal Paradox Basin alluvial fans was sourced from an extremely limited catchment dominated by 1.4-1.5 Ga meta-igneous rocks. In contrast, the medial-distal fluvial strata tapped a wider, potentially axially flowing, catchment and show both the 1.7-1.8 Ga and 1.4-1.5 Ga zircon ages reflecting the broader uplift. Further, we conducted (U-Th)/He analysis to investigate the thermal history of the Uncompahgre Uplift. In doing so we discovered a West to East trend where the western samples, which are closer to the La Sal Mountains, are reset more than the Eastern samples. Probability analysis were performed and preliminary results suggest that Oligocene Volcanism from the La Sal Mountains could cause this west to east trend in ages.

URANIUM-THORIUM-LEAD CHRONOLOGY OF FISH BONE IN PETROLEUM SOURCE ROCKS: AN EXAMPLE FROM THE EAGLE FORD GROUP, TEXAS

SLABIC, A. AND T. J. LAPEN

The U-Th-Pb isotope systematics of TOC (total organic carbon)-rich sedimentary rocks are investigated to test the potential for these isotope systems to record the timing of deposition and periods of diagenesis. The samples investigated for this project were derived from the well-dated Eagle Ford Group (EFG) Shale, located in south-central Texas. The preliminary sample material analyzed for this study is dated at 90.6 Ma based on the astro- and geochronologic age model of Eldrett et al. (2015). In situ analyses of U, Th, and Pb isotope ratios and rare earth element (REE) abundances of fish bone phosphate and carbonate calcispheres were conducted by laser ablation inductively-coupled plasma mass spectrometry (LA-ICP-MS) on materials collected from research core Iona-1. The core, located in Southwest Texas, was drilled by Shell International Exploration and Production Inc. in January 2012. Qualitative major element abundances and sample mapping were conducted by scanning electron microscopy (SEM) and energy dispersive spectroscopy (EDS). The REE data in fish bone indicates significant local REE uptake. The preliminary Th-Pb isotope data yield an age of 92±4 Ma for material analyzed and indicates that the fish bones have retained their original, or very early, diagenetic Th-Pb isotope systematics, making them promising candidates for dating shale deposition. The U-Pb isotope systematics indicate that U was mobilized and greatly enriched in the fish bone after deposition. Preliminary modeling of the U and Pb isotope data points to a short period of U and uranogenic Pb re-distribution at 57 +17/-9 million years ago. This late U mobility may complicate interpretations of U isotope compositions as an indicator of redox conditions.

EVALUATION OF HYPERSPECTRAL CLASSIFICATION METHODS TO MAP AND IDENTIFY MINERAL ALTERATIONS AND STRATIGRAPHIC RELATIONSHIPS IN THE ASPHALT-RICH ANACACHO LIMESTONE TO IDENTIFY FUTURE PROSPECTS

SMITH, V.

The Late-Cretacious Anacacho Limestone is a high-energy carbonate deposit that formed on top of Cretaceous volcanic mounds. The most notable aspects about this formation are the surficial asphalt deposits and sub-surface oil accumulations. The asphalt in the Anacacho Limestone is a combination of hydrocarbons and heterocyclic compounds and since the combination of the rock and asphalt requires no refining, the Anacacho Limestone is being mined as a cost-effective method to produce road-paving materials. Additionally, carbonate formations are some of the largest hydrocarbon-bearing reservoirs in the world. Therefore, understanding the mineral relationships between carbonate rocks and hydrocarbons is very important when trying to identify future prospects through observation and analysis of surface alterations. The purpose of this study is to evaluate and determine the best hyperspectral classification methods to map the outcrops and identify mineral alterations associated with asphalt occurrence using ground-based hyperspectral scans of Anacacho Limestone outcrops. Hyperspectral Imaging is ideal for mapping and identifying minerals and mineral alterations because it uses hundreds of narrow bands that detect subtle changes in spectral response. Additionally, Ground Based Hyperspectral Imaging is particularly useful when observing vertical outcrops that are not able to be scanned by airborne or satellite hyperspectral scans. These cost-effective methods can then be a useful tool to in mapping other outcrops to determine stratigraphic relationships, reconstruct geologic history and identify surficial mineral alterations associated with asphalt to discover future prospects.

USING SUBSIDENCE ANALYSIS TO TEST WHETHER THE EASTERN USA AND NORTHWESTERN AFRICA CONJUGATE MARGINS ARE UPPER PLATE AND LOWER PLATE RIFTED MARGINS

STIBBE, E.

Previous work assigned upper plate-lower plate designation to the central Atlantic conjugate margins in the eastern USA and northwest Africa. Upper plates are recognized from: 1) their thicker and higher-standing, unthinned area of continental crust; 2) their narrow zone of thinned, seaward-dipping continental crust with more restricted hydrocarbon fairways; 3) their fewer and higher-dip, syn-rift normal faults; 4) their lack of post-rift, salt-filled sag basins; and 5) their cross-sectional asymmetry when compared to their conjugate margin. Lower plates, in contrast, are commonly identified by: 1) their thinner and lower-standing crust; 2) their broad area of thinned continental crust commonly overlain by post-rift, salt-filled sag basins; 3) their more expansive, hydrocarbon fairways; 4) their pervasive, lower-dip, syn-rift normal faults; and 5) their cross-sectional asymmetry when compared to their conjugate margin. Various geometries of alternating upper and lower plates have been proposed based on topography, margin curvature, and crustal structure. In general the eastern USA margin has the crustal and topographic character of a single, lower plate margin. To test which plate is the more thinned lower plate vs. the less thinned upper plate, we have compiled well subsidence data from from the deepest penetrating wells on both margins and by using pseudo-wells based on deep-penetrating seismic reflection data. Subsidence data support the eastern margin of the USA as a lower plate margin due to much greater, observed subsidence than observed in northwest Africa. A challenge in northwest Africa is removing the effects of Cretaceous and Cenozoic hotspot activity on the longer term subsidence pattern.

PETROLOGY OF ZIRCON BEARING DIOGENITE NORTHWEST AFRICA TEN THOUSAND SIX HUNDRED SIXTY SIX

TANNER, T. B., C.R. JEFFCOAT, M. RIGHTER, E.L. BERGER, T.J. LAPEN, A.J. IRVING, S.M. KUEHNER, AND G. FUJIHARA

The howardite, eucrite, and diogenite (HED) meteorites are a group of achondrites thought to be derived from the asteroid 4 Vesta. Petrologic, geochemical, and isotopic investigation of the HED meteorite group provides a means of understanding early planetary differentiation processes and early evolution of planets in our solar system. Diogenites can be broadly classiffed as coarse grained orthopyroxenites with some samples containing appreciable amounts of clinopyroxene, olivine, chromite, and plagioclase. Many diogenites are brecciated, however, there are few poorly to un-brecciated samples. Diogenites are important because they may represent the lower crust of 4 Vesta. Orthopyroxene (Fs35Wo2) defines a dominant orthocummulate texture and occurs as larger, subhedral, interlocking grains. Clinopyroxene (Fs14.4Wo43.2) occurs as exsolution lamellae in nearly all orthopyroxene and as discrete grains. Plagioclase (An81.3-86.3Or0.6-3.0) grains are anhedral and irregularly distributed. Grain boundaries between plagioclase and orthopyroxene are locally jagged. A large grain (3-4 mm) of ilmenite hosts several subhedral grains of zircon. Apatite grains are predominately present adjacent to discrete clinopyroxene grains and occur mostly near the large ilmenite grain in the sample. Textural and mineralogical associations indicate that the large orthopyroxene was an early forming phase. The compositions of the pyroxene in the plagioclase-rich areas are compositionally identical to the pyroxenes in the plagioclase poor areas suggesting that these areas are not likely a mixture of distinct lithologies. The ilmenite that hosts the zircons appears to be intergrown in an igneous, not fracture contact with the host orthopyroxene and clinopyroxene.The zircons contained in NWA 10666 represent the first recognized occurrence of this datable phase in a diogenite.The zircons are large enough for in situ analysis of U-Pb isotope compositions and Ti-in-zircon thermometry. Zircon size, Pb diffusion data, and published cooling rate estimates for diogenites yield Pb closure temperatures of 1100-1300 C. Zircon ages are likely to represent the age of igneous crystallization. The phosphate grains are also amenable to U-Pb dating, but have a lower closure temperature than zircon (~500 C). These data would allow us to further evaluate the thermal history of this diogenite.

COMPARISON OF BURIAL HISTORIES, SUBSIDENCE RATES, AND TECTONIC EVENTS ON THE JURASSIC-RECENT DEMERARA-GUINEA CONJUGATE MARGINS, EQUATORIAL ATLANTIC OCEAN

ZAVALA, O.

The Demerara-Guinea conjugate margin records two rift events in the breakup of Pangaea: the Triassic-Jurassic (252-201 Ma), Central Atlantic rifting event between North America and South America in a northwest-southeast direction and the Berriasian-Aptian (201-113 Ma), Equatorial Atlantic rifting event between South America and Africa. I constructed 18 burial plots from 5 wells on the Demerara margin and 13 wells from the Guinea margin to compare their rift and subsequent passive margin histories. The main tectonic events shared on both conjugate margins include: 1) Central Atlantic rift phase (give geologic age, 252 Ma to 145 Ma); 2) Central Atlantic passive margin phase (geologic age, 145 Ma to 112 Ma); 3) Equatorial Atlantic rift phase (geologic age, 112 Ma to 95 Ma); and 4) Equatorial Atlantic passive margin phase (give geologic age, 95 Ma to present day). The events occur slightly earlier by ~56 Ma on the Guinea margin than the Demerara margin. Subsidence rates of 1692.2 cm/Ma (general subsidence rate) on the Guinea margin are faster than observed rates of 236.86 cm/Ma (general subsidence rate) on the Demerara margin. These general subsidence rates are attributed to the presence of the Casamance River delta of Santonian age (86.3 Ma to Present) towards the east of the Guinea plateau.

APTIAN TO RECENT, POST-RIFT COOLING AND SUBSIDENCE HISTORY OF THE SOUTHEASTERN MARGIN OF BRAZIL AND CORRELATION TO LATE CRETACEOUS-CENOZOIC PHASES OF THE ANDEAN OROGENY

ZHANG, L.

The breakup of West Gondwana resulted in the formation of the South Atlantic rifted continental margins during the Aptian these margins are commonly assumed to have subsided as passive margins since the time its Cretaceous rifting. In this senior thesis, I have compiled fission track data from 10 previous authors that is based on outcrops ranging in age from Precambrian to Jurassic that are exposed along the southeastern margin of Brazil. Compilation of 222 fission track data points reveal two main cooling events: 1) Late Cretaceous (100-70 Ma) that is limited to the Serra Domar range; and 2) Oligocene to recent (30-0 Ma) that is regional in scale. As proposed by previous authors, these two events correlate with phases of the Andean orogeny located 2300 km to the west of the study area along the Pacific margin of South America. The farfield transmission of east-west-oriented compressive stress from the Andean Mountains reactivated Precambrian shear zones in the coastal area of Brazil as normal and strike-slip faults, some of which are presently active. The two main periods of fault reactivation occurred during the Peruvian phase of Andean compression in the late Cretaceous (90-75 Ma) and during the later Quechua phase of Andean compression during the Neogene (25-0 Ma). I also constructed burial plots for seven offshore wells in the Campos basin that are located about xx km from the fission track study onland. These burial plots reveal periods of increased subsidence the younger, Oligocene to recent event.

M.S. and Early Ph.D. Students

APPLICATION OF GEOPHYSICAL TECHNIQUES TO STUDY THE INTERNAL ARCHITECTURE OF COASTAL DUNE MORPHOLOGY, NORTH PADRE ISLAND, TEXAS

AGGARWAL, J., S. KHAN, AND J. WELLNER

The Texas coast contains the longest barrier island, Padre Island. Large populations visit the beaches in this area disturbing the natural environments and affecting the ability of the foreshore and dune environments to protect the mainland from erosional events. Sand dunes provide protection from these events due to their location on the highest point of the barrier islands. Dunes absorb the impact of storms, and prevent floods from damaging coastal cities. Coastal dunes in the northern portion of North Padre Island gain sediment through longshore drift from the northeast. In order to help with the erosion, maintained dunes are being constructed and sustained with planting of vegetation on the seaward side along the Gulf Coast. Differences in the internal structure of naturally formed dunes and maintained dunes can provide crucial information on the effectiveness of maintained dunes. The study of coastal dunes on North Padre Island, Texas, provides insight to the benefits of protecting dunes through management programs, as well as effectiveness of maintenance on these dunes. This study utilizes GSSI 3000 and 4000 computers with a monostatic 200 and 400 MHz antenna for subsurface data collection. Penetration ranges from 0 to 4 m and 0 to 2 m, respectively, for these two systems. Vertical resolution is approximately 0.15 m and 0.07 m. Six profiles were collected on two dunes, three perpendicular and three parallel to shore at each site. In the radar profile, the water table is identified by the strong horizontal reflector throughout the survey on the natural dune. Future work includes creating a time lapse to demonstrate the amount of protection these dunes provide in comparison to each other.

SUBSURFACE STRUCTURAL MAPPING AND PETROLEUM SYSTEMS MODELING OF THE PORT ISABEL PASSIVE MARGIN FOLDBELT, NORTHWEST GULF OF MEXICO

BUGTI, M. N.

The Port Isabel passive margin foldbelt (PIFB) of Oligocene age in the northern Gulf of Mexico (GOM) is lesser known from hydrocarbon exploration than its younger, Miocene age, deeper-water neighbor, the Perdido passive margin foldbelt (PFB), because the PIFB has had no commercial hydrocarbon production, while the PFB contains three giant fields with a peak production of 100 kboe/day. In order to better understand this major gap in the hydrocarbon productive zone of the US GOM, I have mapped a grid of 25,000 line km of 2D seismic lines with penetration from 14 to 25 seconds TWT that extends across the from the Texas coastline from the Corsair normal fault zone on the updip end of the PIFB to downdip compressive structures of the PFB in water depths of 2450 meters. My mapping results include: 1) the sharp “corner” in the shape of the NW GOM margin has influenced the evacuation of salt by the process of radial gliding from a amphitheater-shaped area of the outer shelf and slope; 2) this evacuated salt has accumulated as a salt canopy towards the downdip and it also accumulated as cluster of diapirs along the bisector line of the corner; and 3) structurally, the transition is abrupt between the Corsair normal fault zone and the convergent features of the downdip thrust belt. I have generated 1D petroleum systems models based on northwest to southeast-trending 2D lines that pass through the few wells drilling in the PIFB. None of these wells have penetrated source rock intervals so my models for the PIFB assume two, underlying source rock intervals: the Tithonian and Turonian. The PSM model results show that expulsion from both sources started at around 54 Ma and peaked during 50-48 Ma. Expulsion by vertical migration charged reservoirs of Oligocene and Miocene age.

SEISMIC TOMOGRAPHIC CONSTRAINTS ON PLATE-TECTONIC RECONSTRUCTION OF NAZCA SUBDUCTION UNDER SOUTH AMERICA SINCE LATE CRETACEOUS (~80 MA)

CHEN, Y. W., J. WU, AND J. SUPPE

Our understanding of the global plate tectonics is based mainly on seafloor spreading and hotspot data obtained from the present earth surface. However, in convergent tectonic settings vast amounts of lithosphere has been lost to subduction, contributing to increasing uncertainty in plate reconstruction with age. However, subducted lithosphere imaged in seismic tomography provides important information. By analyzing subducted slabs we identify the loci of subduction and assess the size and shape of subducted slabs, giving better constrained global plate tectonic models. The Andean margin of South America is a classic example of continuous subduction up to the present day, providing an opportunity to test the global plate prediction that ~24×106 km2 (4.7% of earth surface) lithosphere has been subducted since ~80 Ma. In this study, we used 10 different global seismic tomographies and Benioff zone seismicity under South America. To assess the undeformed length of subducted slab, we used a refined cross-sectional area unfolding method from Wu et al. (2016) in the MITP08 seismic tomography (Li et al., 2008). Having cut spherical-Earth tomographic profiles that parallel to the Nazca-South America convergence direction, we measured slab areas as a function of depth based on edges defined by steep velocity gradients, calculating the raw length of the slab by the area and dividing an assumed initial thickness of oceanic lithosphere of 100km. Slab areas were corrected for density based on the PREM Earth model (Dziewonski and Anderson, 1981). We found the unfolded length of the Nazca slab is 7000km at 5◦N and gradually decreases to 4700 km at 30◦S, with total area of ~24×106 km2. Finally, we imported our unfolded Nazca slab into Gplates software to reconstruct its tectonic evolution and find that our unfolded base of the Nazca slab fits tightly against South America at ~80 Ma if the pre-deformed South America margin of McQuarrie (2002) is used. This close fit implies a plate reorganization at the South American margin, marking the beginning of Nazca subduction at ~80 Ma. This observation is generally in agreement with geological evidence, illustrating the importance of subducted-slab constraints in convergent plate-tectonic reconstruction.

EARTH INNER CORE ANISOTROPY USING PKIKP AND PKIIKP REFLECTIONS

CHEW, J., Y. ZHENG, AND H. HU

Past research has supported the idea of an anisotropic inner core with the polar axis as the fast axis. There is also an observed fast eastern and slow western hemisphere that is not divided at a 180 degree half. Most inner core research is accomplished through observation of deep seismological, transmitted waves, such as the PKP(DF), with a source-receiver distance of greater than 150 degrees. The differential traveltimes between this phase and other core phases were used to image the anisotropy. However, the separation between the source and receiver created ray path separation in the mantle, which could introduce error in calculations due to small, low velocity mantle zones. This project introduces a new method to study the effects of solely the inner core using reflected PKiKP and PKIIKP waves at a small source to receiver distance (up to about 40 degrees). The small distance is key to minimizing effects of small mantle heterogeneities, providing a more accurate inner core anisotropy picture. Data for this project includes seismograms obtained from IRIS for global earthquakes from 1990 to 2016 of moment magnitudes 6.1-6.5. Seismogram data is loaded into a Matlab GUI program from which pairs can be saved. Theoretical phase traveltimes calculated from iasp91 velocity model are plotted in the GUI program to aid in choosing the correct phases. This project will look at the whole inner core anisotropy.

INVESTIGATING GROUND SURFACE DEFORMATION: EXAMPLE FROM THE HOUSTON AREA

CRUPA, W. E.

The Houston area has undergone significant ground deformation in the last century, with the main factor being attributed to groundwater and natural gas withdrawal induced subsidence. However the Houston area, like most of the Gulf Coast, is also home to many faults and situated above numerous slow moving salt diapirs. The effect that these two contributing factors have had on ground deformation has not previously been studied in depth. This means that horizontal components of ground motion have been largely ignored in scientific studies and when making policies to alleviate ground surface deformation. In this study, we investigate the contributing effects of salt domes to the overall ground surface deformation in the Houston area by:1) Processing and rotating GPS data in the Houston area into a fixed North American reference frame to see the true horizontal and vertical velocity vectors; 2) Modeling changes in the water table and correlating GPS rates with ground and surface water data from 1990-2017; 3) Assessing surface deformation using SBAS InSAR processing technique over the Houston area.

ELASTIC WAVE IMAGING USING P-P, SH-SH, AND SV-P EVENTS: MODELING AND DATA PROCESSING

ERMOLAEVA, E. AND R. R. STEWART

There is a growing interest from the oil and gas industry towards unconventional processing methods that allow lowering the cost of seismic surveys. One of the most intriguing concepts is building additional subsurface images using “secondary” wave modes present in the existing “legacy” seismic data sets. Earlier, these “secondary” wave modes were considered undesirable and were removed to improve the image of the primary waves. Now, the work is being done to extract them from the conventional single component seismic data using various algorithms and processing techniques. This work is concentrated on using the “V-V” seismic data (converted compressional waves (SV-P) generated by the vertical vibrator along with the primary compressional waves (P-P) and then recorded by the single vertical geophone) to build subsurface images. These recorded waves are separated from each other using conventional data processing techniques and analyzed independently yielding results similar to a conventional converted wave seismic method without a 3C receiver. Theoretical analysis and elastic modeling are used to determine character of propagation and strength of the SV-P waves. Special processing flow is created to allow careful noise attenuation while keeping low frequency SV-P signal intact to obtain robust P-P and SV-P images upon separation. Original “V-V” dataset and an additional pure shear (SH-SH) dataset are also processed to obtain P-P and SH-SH images and their corresponding velocity fields. The resulting images are compared to study the differences and similarities between them as well as the subsurface details. Despite several drawbacks that include strict limitations applying to the legacy seismic data, lack of special pre- and post- processing procedures for SV-P waves, and potential absence of any supporting shear wave information that could help with the processing, it is determined that it is possible to build a robust complimentary SV-P image and extract the shear wave information using only “V-V” data. This would allow performing a full-wave analysis of the existing data without the need to fund any additional converted or pure shear wave surveys.

GREEN'S FUNCTION IN VISCOELASTIC MEDIA

GHOSH, A.

The Green's function in Viscoelastic media is calculated taking the Complex Stiffness tensor into account.

BURIED GLACIAL GEOMORPHIC FEATURES ON EROSIONAL SURFACES USING 3D SEISMIC DATA IN THE SOUTHWESTERN BARENTS SEA, ARCTIC NORWAY

KONG, J.

Identifying buried, glacial geomorphic features can aid in developing a better understanding of past Arctic ice sheet behavior. The Barents Sea, a marginal sea off of northern Norway and Russia, covers one of the world's widest continental shelves, with an average water depth of 230 meters. Over the last 3.5 million years, the growth and retreat of ice sheets on this shallow continental shelf have significantly changed the bathymetry of the Barents Sea. Glacial erosion was particularly concentrated around 1.0 Ma, when multiple ice sheets converged and completely covered the Barents Sea for the first time. During this period of convergence, flowing ice beneath the ice sheets eroded sediments and carved features into the substrate, such as mega-scale glacial lineations, ploughmarks, and transverse ridges. As the ice sheet retreats, new sediment is deposited over the formerly ice-covered surface, preserving these glacially-carved features. Identification and analysis of these preserved features, found beneath the modern day seafloor, can illustrate past ice sheet characteristics before the Last Glacial Maximum, such as ice flow direction or areas of ice sheet retreat. This study aims to use the interpretation of densely-spaced 2D seismic data (1-5 km) to map the regional extent of glacial unconformities formed during periods of ice growth. More detailed interpretation from 3D seismic grids, covering ~7400 km2, will make higher resolution interpretations that will allow for the identification of features buried below the seafloor on the unconformity formed during the onset of glaciation. This interpretation will identify and examine glacial features that are up to 800,000 years old in order to better understand glacial behavior in the Arctic. Further work will include measuring the slopes and geometries of glacial features, which could ultimately be related to similar features found in other glacial environments. Comparison of Arctic and Antarctic geomorphic features, formed during glacial periods, could help to better understand the processes that generate subglacial geomorphic features.

NEW OBSERVATION ON SEISMIC ANISOTROPY IN SUBDUCTING SLABS INFERRED BY NON-DOUBLE COUPLE EARTHQUAKE RADIATION PATTERNS

LI, J., Y. ZHENG, L. THOMSEN, T. LAPEN, AND X. FANG

Nearly one third of earthquakes are deep earthquakes with focal depths exceeding 60 km. Most of them occur in subduction zones and show non-double-couple (non-DC) radiation patterns. Previously, this non-DC radiation pattern was explained in an ad hoc fashion event by event. However, in this work, we found that these non-DCs could be satisfactorily explained by assuming that (i) all earthquakes are shear dislocation faulting but (ii) they are embedded in a common but tilted transversely isotropic (TTI) medium. The TTI anisotropy is characterized by the symmetry axis (two angles) and 3 Thomsen parameters among which the S-wave anisotropy is best resolved by our algorithm. The S wave and P wave velocities parallel to the symmetry axis are derived from the preliminary reference earth model (PREM). We used the centroid moment tensors (CMT) from Harvard's catalog to invert for both the TTI symmetry axes and anisotropy strengths for global subduction zones: Tonga, Java, Molucca, Vanuatu, Mariana, Japan, Kuril, and Aleutians. Our inversion results show that in nearly all studied regions (19 earthquake groups) the TTI symmetry axes are perpendicular to the subducting slab interface but with a few (3 earthquake groups) exceptions where several deep-focus regions have symmetry axes parallel to the subducting slab interface. For all subduction zones and for all depths (100km to 650km), the inverted S-wave anisotropy has a typical value of about ~28% (ranging from ~6% to ~46%) and we observed no clear dependence on depth. This shows that the rock fabrics hosting the intermediate-depth and deep-focus earthquakes are no different, pointing to a possibility that there is no difference between intermediate-depth and deep-focus earthquakes in terms of their mechanisms. Our anisotropy observation is independent of slab subduction rate, age, and dip angles, etc. Given the global nature of our observation, we postulate a common process in all subduction environments. Such a process may be the metamorphic reactions in the slab, which can generate sheet silicates and layered fabrics. Our inverted anisotropy provides important information on mechanisms of the intermediate-depth and deep-focus earthquakes.

BASEMENT AND CRUSTAL STRUCTURE OF JURASSIC OCEANIC CRUST IN THE EASTERN GULF OF MEXICO

LIN, P.

An extinct ridge-transform plate boundary extends 1,500 km in an arcuate pattern from southwest to northeast across the deepwater area of the Gulf of Mexico. This extinct ridge that is buried beneath 5-7 km of Jurassic to recent sedimentary rocks was first imaged in its entirety by previous workers using satellite-derived, vertical-gravity, gradient data. I used 25,000 km2 of deep-penetration seismic reflection data from the oil industry to map the top of oceanic crust and its Moho in the eastern Gulf of Mexico (EGOM) between the Florida and Yucatan Peninsulas. My mapping reveals that the EGOM oceanic ridge system is defined by 30-60-km-long segments of axial valleys bounded by inwardly-facing normal faults and occupied by axial volcanoes up to 15-km-wide and up to 2 km in vertical relief in an appearance characteristic of modern, slow-spreading ridges. Based on the depth of the Moho mapped from the seismic reflection data, I interpret a 50-6.7-km-thick, oceanic crust beneath spreading ridge segments that is expressed as negative, free-air, bullseye-shaped gravity anomalies. The central location of the axial volcanoes on all four of the axial valley segments indicates a decreasing magma supply near the ends of each spreading segment that is characteristic of modern, slow-spreading centers. My mapping of the area of oceanic crust and its landward limits along the continent-ocean boundaries of the Florida and Yucatan conjugate margins indicates that spreading on this ridge is asymmetrical with 150 km of oceanic crust on its northern limb and 80 km on its southern limb. Previous work by Imbert (2005) mapped a possible, east-west axial valley that is possibly a spreading ridge that predated the one I mapped in detail to the south. A late Jurassic, spreading ridge jump from the older, shorter-lived spreading ridge in the north to the longer-lived spreading ridge I mapped in detail to the south may account the greater width by 70 km of oceanic crust in the north.

COMPARISON OF THE SUNDA SLAB FROM MITP08 TOMOGRAPHY AND MANTLE FLOW MODELS: IMPLICATIONS FOR PLATE TECTONIC RECONSTRUCTIONS OF SOUTHERN SUNDALAND SINCE THE CRETACEOUS

LIN, Y. A., J. WU, AND N. FLAMENT

Published plate tectonic reconstructions of southern Sundaland and the Sunda trench, southern Indonesia, since the Cretaceous remain highly variable and controversial. Two very different end-member models have been proposed that each predict very different subducted Sunda slab structures and mantle temperature fields. The model of Hall (2012) envisioned a transform between the Indian and Australian plates from 90 to 45 Ma and predicted a relatively short subducted Sunda slab. In contrast, Whittaker et al. (2007) predicted a subduction of the Wharton ridge, which implied a longer subducted Sunda slab and potential slab window. In this study, we will test the viability of the Whittaker et al. (2007) plate model by first mapping the Sunda slab structure from MITP08 tomography Li et al. (2008). We then compared our mapped Sunda slabs to a predicted Sunda slab structure from a published CitcomS mantle flow model Flament et al. (2017) that included the Whittaker et al. (2007) plate model as input. Differences between the mapped and modeled Sunda slab structure included: (1) At the Java trench, our mapped Sunda slabs from MITP08 tomography dip northwards down to 1000 km depths. In contrast, the modeled Sunda slabs show a reversal from northward to southward dips at 500 km depths. (2) At the northwest Sumatra trench, our mapped slabs from tomography showed a conspicuous gap between the upper and lower Sunda slabs at 700 to 800 km depths. In contrast, modeled Sunda slabs were continuous down to 1300 km depths. We will discuss the differences between mapped and modeled Sunda slab structures with the aim of improving the plate reconstruction model for southern Sundaland since the Cretaceous.

GRAVITY MODELING AND SEISMIC REFLECTION STUDY OF THE BARREIRINHAS AND CEARA BASINS OF NORTHERN EQUATORIAL BRAZIL

LUNN, E.

The Barreirinhas and Ceara Basins of offshore northern equatorial Brazil cover a combined area of approximately 105,000 km2 and form the northern and southern flanks, respectively, of the Romanche Fracture Zone (RFZ). The RFZ is a linear fracture zone with an average width of approximately 16 km that extends over 4500 km from offshore northern equatorial Brazil to its conjugate margin near offshore Ghana and Togo/Benin. The Barreirinhas basin exhibits characteristics of a less-extended, upper plate margin including a steeper and more abrupt continental margin and high free-air gravity reflecting a shallower and thicker basement and thick sedimentary fill. In contrast, the Ceara basin south of the RFZ exhibits characteristics of a more-extended, lower plate margin including a gently sloping and wider continental slope and a low free-air gravity reflecting a deeper basement and thinner sedimentary infill. The conjugate margins in West Africa are reversed over the RFZ; lower plate Ghana faces upper plate Barreirinhas and upper plate Togo/Benin faces lower plate Ceara. Lower plate margins, such as the proposed Ghana and Ceara margins, have been found to be more suitable environments for hydrocarbons due to greater sedimentary thicknesses, wider fairways, and higher heat flows than upper plate margins. This conclusion is supported by the 2007 discovery of the Jubilee field within the lower plate Ghana margin and the 2012 discovery in the Pecem deepwater well within the lower plate Ceara margin. The Barreirinhas is a frontier basin with several small gas wells and no deepwater discoveries. Gravity transects across both basins were made parallel to the RFZ and validated with existing seismic refraction and reflection data to show variations in extension that is supportive of the upper plate-lower plate hypothesis.

INVESTIGATION OF THE INFLUENCE OF PLANETARY BOUNDARY LAYER EVOLUTION AND METEOROLOGY ON AIR QUALITY IN MEXICO CITY

OSIBANJO, O. AND B. RAPPENGLUECK

The evolution of the planetary boundary layer (PBL) is critical to air pollution studies as it impacts the concentration of pollutants in the lower troposphere. Pollutants emitted at the surface are being trapped and raised to unhealthy levels within the PBL during stable atmospheric conditions. In addition to the impact of PBL evolution on air quality, meteorology also plays a major role, especially when a high-pressure system (associated with warm, clear sky conditions) is present. This enhances the formation of ozone as insolation is strong during such atmospheric conditions. This study investigates the specific meteorological conditions in the Mexico City basin associated with poor air quality conditions. Mexico City usually experiences three seasons, which are the cold dry season (November-February), the warm dry season (March-April), and the rainy season (May-October). The ozone season usually occurs during the warm dry season. The objective of this study is to estimate the PBL height using the parcel method based on the potential temperature profiles measured continuously by a MP-3000A microwave radiometer and wind speed and direction data up to 3-5 km agl by a 915 MHz RAPTOR radar wind profiler during two weeks in March 2016 from a monitoring site in Mexico City. Both instruments were deployed and maintained by SEDEMA (Secretaría del Medio Ambiente), the Environment Department of the Mexico City Municipality. It has been the most severe smog episode since 2007.

QUANTITATIVE ANALYSIS OF SILICICLASTIC CLINOFORMS AN EXAMPLE FROM THE NORTH SLOPE ALASKA

RAMON-DUENAS, C., K. W. RUDOLPH, P. EMMET, AND J. S. WELLNER

2D seismic lines from the US Geological Survey (USGS) public database from onshore northern Alaska and 52 wells were used to study the stratigraphic evolution of the Lower Cretaceous Brookian sequence. This sequence is composed of thick, prograding clastic deposits that originated from the ancestral Brooks Range thrust, filled the Colville foreland basin, and overstepped the Beaufort rift shoulder. In particular, this study focused on the foresets and topsets of the Torok and Nanushuk Formations of Lower Cretaceous age which are well-recognized for large-scale clinoforms with depositional relief on the order of 400 to 600 m. In the area of National Petroleum Reserve Alaska (NPRA), we utilized approximately 5700 km of seismic data from the 1974-1981 vintages which was post-stack reprocessed in 2000. In the area of Colville River to Prudhoe Bay, a non-migrated 1980 vintage was used, with 5600 km of seismic data. 52 wells throughout the area with Gamma Ray, Resistivity, Density and Sonic logs were used. We interpreted and mapped eighteen progradational surfaces. Slope shapes and geometries were described, and relative qualitative relations were established for the topset and foreset volumes. Ongoing work on stratigraphic well description and seismic well ties will lead to a better understanding of slope relations and rock types. The Torok- Nanushuk clinoforms prograde from west to east-northeast. The thickness of each section of the sequence varies, reflecting changes in accommodation from the foredeep part of the basin into the rift shoulder. The geometry of the clinoforms and the foreset-topset volume relations suggest that more sediment volume was deposited on the slope (delta front) rather than on the shelf. Previous investigators have reported that average slopes vary from 0.6 to 2.5 degrees with maximum dips of 10 degrees. Understanding the relationship between slope geometries and clinoform sediment volume is imperative for the recognition of basin evolution, asymmetry, and tectonic processes. The NPRA area provides a unique setting for the characterization and comparison of sedimentary volumes and depositional slopes and allows meaningful comparisons to other basins.

2D SEISMIC CHARACTERIZATION OF THE MESOZOIC CARBONATE PLATFORM, OFFSHORE GUINEA-BISSAU, SENEGAL BASIN, NW AFRICA: TECTONIC IMPLICATIONS

SERRANO-SUAREZ, B. E.

During the Jurassic-Early Cretaceous, a continuous, carbonate platform developed along the margin of northwest Africa. This study uses 14,812 km of 2D seismic data tied to six exploration wells from the offshore Guinea-Bissau, Senegal Basin - provided by First Exchange Corporation and Spectrum - to describe the carbonate platform. I mapped four horizons: Jurassic, Aptian, Albian, and Santonian. All horizons, except for the Jurassic, were tied to exploration wells in the area. The Jurassic was tied with the DSDP 367 well. The carbonate platform offshore Guinea-Bissau exhibits subparallel, low- to high-amplitude reflectors bounded to the west by a strong, irregular, high reflectivity event interpreted as an erosional unconformity or collapse scar. Reflectors to the west onlap against this surface. In the eastern area, the carbonate platform lies conformably beneath younger, clastic sequences. Well data indicate a gradual increase in clastic input to the carbonate platform starting in the Albian. The Aptian section consists of micritic limestone and dolomite, with minor shale and sandstone and is interpreted as the top of the carbonate platform. In the southern area, this top of the carbonate platform is less well constrained. In the northern area, the Santonian horizon truncates the Aptian and Albian and locally truncates the Jurassic. In the central area, the Aptian truncates the Jurassic, and the Santonian locally truncates the Aptian. In the southern area, the Albian truncates the Aptian. These varying areas truncations indicate that the northern part of the carbonate platform was eroded during the Santonian and the southern part of the carbonate platform was eroded during the Albian. I use these data to compare to existing tectonic models for the NW African carbonate platform that include: 1) a model related to the farfield, compressive stress transmitted by the Africa-Europe collision; and 2) a model related to transpressional motion along the South America-Africa plate margin.

IDENTIFICATION OF SWEET SPOTS FOR HYDRAULIC FRACTURE IN AVALON SHALE, PERMIAN BASIN, USING LITHOFACIES CLASSIFICATION

SOURI, Z.

Kerogen content and brittleness are the most important factors for investigating unconventional resources. Sweet spots for hydraulic fracture are marked by high kerogen content (high TOC) and high brittleness. A 2-D depth section of sweet spots is made using lithofacies classification in Avalon Shale, within the Delaware Basin of the Greater Permian Basin. This work takes advantage of well-log analysis, artificial neural network and Sequential Gaussian Simulation (SGS) to make a 2-D depth-section of lithofacies between two wells. The proposed methodology might be helpful in sweet spot identification. Development in the Permian Basin has been mostly vertical in the past. During the last couple of years, however, companies have concentrated on horizontal development. Avalon Shale is an unconventional shale unit, which is a sub-unit of the Bone Spring formation in the Delaware Basin. Due to low permeability, unconventional reservoirs need to be artificially stimulated to produce hydrocarbons. It is important to locate spots that are well responsive to hydraulic fracture, which are marked by high organic content (or high TOC) and high brittleness. Well-log analysis is done on two wells (A and B) in the Delaware Basin to mark the zones of interest. TOC and Brittleness are estimated at the location of the two wells and calibrated to core measurements. Well log data is used to build a shale lithofacies model at the well A, and then an artificial neural network (ANN) is used for lithofacies prediction at the well B. Four petrophysical parameters derived from conventional logs: density, sonic, gamma ray and resistivity were determined as critical inputs. An SGS is then used to create a 2-D depth section of lithofacies, and ultimately sweet spots for hydraulic fracture in between the two wells.

LATE JURASSIC STRATIGRAPHIC AND STRUCTURAL EVOLUTION OF THE NORTHERN YUCATAN MARGIN

STEIER, A.

The Norphlet Formation is a highly productive, well-sorted, quartz-rich, sand unit deposited as late Jurassic sand dunes across the present-day areas of Mississippi, Alabama, Florida, and the deepwater northeastern Gulf of Mexico (GOM). The high porosity and permeability of its eolian reservoir sands and the quality of its source and seal in the overlying Oxfordian lime mudstones of the Smackover Formation are key components of many of the major hydrocarbon discoveries in the northeastern GOM over the past 40 years. My study makes use of nine wells from the western, southeastern, and northeastern GOM tied to published regional seismic lines and 134,000 km2 of 2D seismic data along the northern Yucatan margin to constrain the stratigraphy of the northern Yucatan margin and make detailed comparisons between the present structural setting and thicknesses of evaporite, Norphlet, and Smackover units on both conjugate margins. In the northeastern GOM, thickness of eolian Norphlet facies exceeds 300 m onshore and 100 m in deepwater settings. The structural setting of the Norphlet Formation ranges from a broad, undeformed platform in central Mississippi to deepwater areas 250 km offshore near Destin Dome and Desoto Canyon that have undergone gravity sliding of the late Jurassic section. This study maps a Norphlet-equivalent sandstone on the northern Yucatan margin adjacent to wells in the Campeche shelf area producing from Oxfordian eolian reservoirs that has a seismic character similar to the deepwater Norphlet Formation of the northeastern GOM. Thicknesses of these discontinuous Norphlet-equivalent units are about 100 m and are associated with a large detachment that dips northward from the Yucatan platform and the Campeche salt province. These structures have been tectonically reconstructed to their locations at the time of late Jurassic deposition by closing the oceanic area of the GOM and reveal a potential single, previously-continuous, northwest-to-southeast-trending region of Norphlet deposition. This period of Jurassic sand dune deposition preceded the Oxfordian initiation of seafloor spreading in the northeast GOM. The presence of a Norphlet-equivalent sandstone with high reservoir quality on the northern Yucatan margin could expand the reservoir fairway by 6,000 km2 in this underexplored region.

IMPACTS OF CENTRAL AMERICAN FIRES ON OZONE AIR QUALITY IN TEXAS

WANG, S. C., Y. WANG, R. LEI, AND R. TALBOT

Background ozone represents the portion of ozone level in one daythat cannot be reduced by local emission controls. One of the important factors causing high background ozone events is wildfires. Satellite observations have documented frequent transport of wildfire smoke from Mexico and Central America to the southern US, particularly Texas, causing haze and exceedance of fine particle matters. However, the impact of those fires on background ozone in Texas is poorly understood. In this study, the impact of the Central America fire emissions in spring (Apr-May) from 2000 to 2015 on Houston-Galveston-Brazoria (HGB) background ozone concentration is investigated and quantified. We first examine through back trajectory analysis to define the fire-impact days of HGB regions which were suffer from the pollutant from Central American fires. The GEOS-Chem global chemical transport model and its nested-grid version over North America are used to simulate the periods of the selected cases studies of Central American fires. Long-large transport of gaseous emissions (NOx, VOCs, and CO) from Central American fires are simulated and satellite observation of these species were also analyzed to investigate the chemistry in long-range transport of Central American fires plumes. Finally, this study quantifies the contribution of fire emissions from Central America on HGB ozone air quality.

ANTI-ALIASING FILTERS FOR DERIVING HIGH-ACCURACY DEMS FROM TLS DATA: A CASE STUDY FROM FREEPORT, TEXAS

XIONG, L., G. WANG, AND P. WESSEL

Terrestrial laser scanning (TLS), also known as ground-based Light Detection and Ranging (LiDAR), has been frequently applied to build bare-earth digital elevation models (DEMs) for high-accuracy geomorphology studies. The point clouds acquired from TLS often achieve a spatial resolution at fingerprint (e.g., 3 cm×3 cm) to handprint (e.g., 10 cm×10 cm) level. A downsampling process has to be applied to decimate the massive point clouds and obtain manageable DEMs. It is well known that downsampling can result in aliasing that causes different signal components to become indistinguishable when the signal is reconstructed from the datasets with a lower sampling rate. Conventional DEMs are mainly the results of upsampling of sparse elevation measurements from land surveying, satellite remote sensing, and aerial photography. As a consequence, the effects of aliasing caused by downsampling have not been fully investigated in the open literature of DEMs. This study aims to investigate the spatial aliasing problem of regridding dense TLS data. The TLS data collected from the beach and dune area near Freeport, Texas in the summer of 2015 are used for this study. The core idea of the anti-aliasing procedure is to apply a low-pass spatial filter prior to conducting downsampling. This article describes the successful use of a fourth-order Butterworth low-pass spatial filter employed in the Generic Mapping Tools (GMT) software package as an anti-aliasing filter. The filter can be applied as an isotropic filter with a single cutoff wavelength or as an anisotropic filter with two different cutoff wavelengths in the X and Y directions. The cutoff wavelength for the isotropic filter is recommended to be three times the grid size of the target DEM.

TRACE ELEMENTS CHARACTERIZATION OF PLAGIOGRANITES FROM BAY OF ISLANDS OPHIOLITE, NEWFOUNDLAND, CANADA

YAN, W., J. F. CASEY, Y. GAO, AND L. LI

In total, six high silica (SiO2>55%) plagiogranites, which are collected from Bay of Islands Ophiolite, Newfoundland, Canada are analyzed for trace elements by using QQQ-ICP-MS. Trace element patterns, including the rare earth elements (REEs) are compared with other similar rocks, for example, from Oman. We hope to summarize their rare earth element patterns and then address their likely petrogenesis process. Some prior studies of the BOIC at UH were primarily limited by the instrument precision and elements detection limit. For example, subject to the instruments XRF, Carter et al. (1985) only measured 6 trace elements of 74 samples in the same area. Therefore, in this study, QQQ-ICP-MS whose detection limit can reach ppt levels was employed to detect 52 trace elements. According to preliminary research completed thus far, these six samples can be classified into 3 different groups, which may then be related to different origins. Group 1: two of these rocks may share same sources since they have very similar REE patterns, demonstrating highly light REE (LREE) and slightly heavy REE (HREE) enriched with obvious negative Eu anomalies. Group 2: rock also has obvious negative Eu anomaly, but has flat LREE pattern and relative high HREE enrichment relative to the LREE. Group 3: No Eu anomaly is observed in last three rocks and their patterns are relatively flat. These patterns are all quite different from the well-known shapes in other ophiolites, such as Oman. In addition, compared with continental crust, all these rocks have very low concentrations of mobile elements but relatively high values of immobile elements when normalized to N-MORB, with opposite negative Pb anomalies in Group 1 while similar Pb positive anomalies in Group 3. Further studies, such as U/Pb age dating of zircons by LA-ICP-MS and major elements analysis by ICP-OES, will be completed to determine more precisely their sources and petrogenesis.

ADVANCED GRADUATE STUDENTS

GROUND-BASED HYPERSPECTRAL STUDY OF A TIDAL INFLUENCED CHANNEL, CRETACEOUS FERRON SANDSTONE, UTAH

BHATTACHARYYA, P. AND S. D. KHAN

A late stage valley fill of the Ferron Sandstone in Central Utah was evaluated by ground-based hyperspectral images. For this study, approximately 45m long, vertical, well exposed outcrop was scanned with both shortwave and visible near infrared specim hyperspectral cameras. This outcrop is mostly characterized by thin layers of shale and sandstone in an interbedded succession on both side of the channel-fill. Electromagnetic radiation reflected from the outcrops is recorded by the hyperspectral sensors. Each material has its own characteristic spectrum. Spectral signature of each pixel is a function of the mineralogy, chemistry, surface alteration, grain size and cements. Spectral signature was used here to distinguish between shale and sandstone within this interbedded succession. Shale has been classified based on the distinctive characteristics of the absorption features of clay minerals within it, such as kaolinite crystallinity index. This interbedded succession has been interpreted as a tidal-influenced fluvial channel fill in a late-stage valley fill. These tide influenced channel deposits represent outcrop analogs useful in the reservoir characterization of heterogenous tide influenced reservoirs.

A REVISED FLEXURAL MODEL FOR THE FORELAND LLANOS BASIN OF COLOMBIA: INDICATION OF AN EARLIER ANDEAN UPLIFT AND ITS HYDROCARBON IMPLICATION

CARVAJAL, L. C.

The Llanos foreland basin (LFB) located eastern Colombia, South America was formed by the interplay of downward forces (tectonic and sedimentary loads) caused by the subduction of the Nazca plate beneath of the South American plate. The uplifting of three cordilleras (Western, Central, and Eastern) since the Late Cretaceous indicates the creation of complex distributions of the sedimentary thicknesses and unconformities in response of bending caused by crustal loads. The aim of this paper is to simulate four flexural models: Late Oligocene (~28.4 Ma), Middle Miocene (~11.6 Ma), Late Miocene (~7.2 Ma), and present day that explains the evolution of the LFB. The mechanical modelling consist of the application of main parameters such as paleogeographic evolution of northern South America, retro-deformational models for the LFB, and topography of the current Cordilleras in which the position, size of the loads, load density, infilling density and flexural rigidity used in the flexural models are directly dependable of the previous considerations. Main results highlights the observations done by previous authors in the LFB where 3D flexural models show that 1) the Llanos basin is a foreland basin is originated by the loading of three Cordilleras since the Late Cretaceous. 2) A foredeep, forebulge and backbulge are identified associated to the LFB through time. 3) Migration of the tectonic bulge produced by the load of the Western, Central and Eastern Cordilleras start since the Late Oligocene toward the East. Maximum displacements of the bulge correspond to ~330 km in the central segment of the basin; therefore, a wider basin is expected in the central part of the LFB. 4) A narrow basin in the south is caused by the concentration of extra loads from the Central Andes where maximum depths of the basin ranges between 6,000-7,000 mbsl. 5) An earlier Late Oligocene thrust-front loading event followed by a bulge migration triggered the first hydrocarbon generation pulse in the LFB; later on, a second bulge migration triggered a Late Miocene hydrocarbon generation pulse.

ASSESSING EFFECTS OF SULFATE MINERALS ON GAS GENERATION IN SHALE USING HYDROUS PYROLYSIS

CHEN, X. AND C. XIAO

Evaporite minerals (including gypsum, anhydrite) containing sulfates as one common group of minerals associated with organic matter can be present in both source rocks and seal rocks. The knowledge of their detailed effects during the formation processes of oil and natural gases is still lacking. In this study, a series of hydrous pyrolysis experiments have been conducted using shale source rocks with different abundances of gypsum (0, 0.3, 0.5, 1 wt.%). The experimental temperature was 330℃ and the duration was 72 hours. The results of chemical composition analysis following experiments have shown that the amount of generated CO2 increases from 70% to 87% of the overall C-bearing compounds with the abundance of gypsum being 0% to 1%. The amounts of light straight chain hydrocarbons (C1 to C3), however, decrease with gypsum. All the light hydrocarbons and CO2 except propane get isotopic heavier with more gypsum. The presence of gypsum provides an oxidizing condition under which hydrocarbons, methane and ethane, in particular, are oxidized to CO2, leading to higher percentages of CO2 and higher 13C values. While the carbon isotope values of C2 and C3 have been used as an effective tool to evaluate maturation of source rocks, the necessary adjustment has to be made to incorporate the reduction-oxidation condition which is caused by the existence of sulfate minerals.

ANALYSIS OF SOLAR-INDUCED FLUORESCENCE (SIF), CARBON DIOXIDE, AND PRECIPITATION USING OCO-2 AND TRMM

CORBETT, A.

In a new age of reliable satellite data, tracking and observing carbon dioxide from space is happening at higher resolution and accuracy than ever before. OCO-2 is one of those satellites. Understanding carbon dioxide sources and sinks is important to understand the role of CO2 in climate change. Additionally, we can now use satellite data to yield a quantitative study of satellite CO2 and in situ measurements to understand the interaction between the biosphere and the atmosphere. Solar-induced fluorescence (SIF) represents the vegetative photosynthesis process and is used to investigate CO2 contributions from the biosphere. SIF data from OCO-2 is compared to TRMM precipitation data. It is found that when SIF, or photosynthesis, is high there is more precipitation. Additionally, high SIF usually means low CO2 in the atmosphere; therefore, there are less atmospheric CO2 when SIF is high in summer. In this study, we found there is a negative correlation between CO2 difference and SIF. With new SIF data, results in this analysis will aid in the greater understanding of the carbon cycle, carbon sources and sinks, as well as carbon dioxide's role in anthropogenic climate change.

MEASURING SPINEL TRACE ELEMENTS IN RESIDUAL MANTLE PERIDOTITE: AN ANALYTICAL PROTOCOL

GHOSH, T. AND J. SNOW

Spinel, being the most resistant phase in residual mantle peridotites, is less affected by mantle processes, e.g., partial melting or refertilization. Thus, it preserves the history of mantle melting events. Therefore, it is essential to find out the trace element signature of spinel along with its major element composition. In this study, we present the analytical difficulty and success encountered during the spinel trace element measurement as well as the protocol for analyzing trace elements of spinels in petrographic thin sections with a thickness of 30 µm. Three out of four samples in this study are extremely depleted peridotites and hence the amount of Ti measured with an electron microprobe was lower than the sensitivity of the probe for those samples, making the coefficient of variation of Ti data much higher than expected. To overcome this limitation, those thin sections were measured in quadrupole ICP-MS. As the sensitivity of the ICP-MS depends on mass, this study was focused on higher masses. Elements to be analyzed were chosen by doing some initial laser ablation analyses on the samples and observing the peak position compared to the background. Mg25 was set to be the internal standard to avoid any potential overlapping. NIST 610 was used as primary standard. Initially, high repetition rate (20Hz) resulted in drilling through the sample and exposing the glass behind as the thin sections were only of 30 µm. Also, changing the repetition rate to a lower value (5 Hz) and a burst of 150 yielded data with higher standard deviation than expected. Eventually, a repetition rate of 10Hz, 100 µm spot size, a burst of 300, 20 seconds of background measure and a wash-out time of 60 seconds resulted in data with coefficient of variation between 0.01-0.1 for most of the elements and yielded a nice, smooth trace element pattern.

TECTONIC ORIGIN OF THE TOBAGO-BARBADOS RIDGE AND TOBAGO FOREARC BASIN BASED ON INTEGRATION OF GRAVITY MODELS AND SEISMIC REFLECTION DATA

GOMEZ, S.

The north-south-trending and 20-60-km-wide Tobago-Barbados ridge (TBR) of the southern Lesser Antilles subduction margin extends 250 km from its southern end on the island of Tobago to its northern end on the island of Barbados. At the southern end of the TBR in Tobago, outcrops of meta-sedimentary and meta-igneous rocks have been interpreted as an early Cretaceous primitive island arc overlain by a late Cretaceous island arc sequence. At the northern end of the TBR in Barbados, exposed rocks are a highly deformed, entirely sedimentary, accretionary prism thought to represent an outer-arc high formed during the Paleogene as part of the nascent Barbados Accretionary Prism (BAP). In this study, I integrate gravity data, well constraints, seismic reflection and refraction data to better understand the crustal structure and tectonic mechanism of the along-strike compositional variation in the crust of the offshore TBR as suggested by its two exposed endpoints. Recent satellite-derived gravity grids were enhanced and filtered to identify the deeper crustal geometry and composition of the TBR. The southern TBR forms a single, bathymetric ridge characterized by a strong and continuous, positive gravity anomaly. At 12.5N, the TBR divides into two bathymetric ridges oriented northeast-southwest both characterized by a moderately-high gravity amplitude anomaly. Two models of ~120-200-km-long gravity transects constructed across the strike of the TBR and one 500-km-long transect constructed along the strike of the TBR reveal the presence of a wedge of high-density crystalline basement at a depth of 14-24 km overlain by ~5 km of meta-sedimentary and meta-igneous rocks and 8-10 km of accretionary prism sedimentary cover. We propose that this wedge of material is composed of difficult-to-subduct Cretaceous, metamorphosed arc crust similar to that exposed on the island of Tobago. The arc type crust has become lodged directly above the subduction trace during westward subduction and was subsequently deeply buried. Uplift of the wedge along thick-skinned, inwardly-dipping thrust faults has elevated the overlying TBR from Middle Miocene to recent time.

CHARACTERIZATION OF FAULTS USING SEISMIC ATTRIBUTES FROM 3D SEISMIC DATA IN THE BAKKEN FORMATION

JAHAN, I., J. CASTAGNA, AND M. MURPHY

The success of horizontal drilling in unconventional oil and gas reservoirs mostly depends on optimal well placement which creates a large number of closely spaced fractures and thus achieves maximum reservoir contact area. Hence, it requires the operator to factor the dominant trend of the natural faults and fractures. Intersecting and crossing conjugate normal faults, ranging from microscale and mesoscale to macroscale are commonly observed in many oil fields. At smaller scales, such faults are a major factor in the development of permeability anisotropy. So, it is highly important to understand the distribution of such faulting in unconventional reservoirs such as the Bakken Formation where permeability is one of the main keys to successful production. A variety of dip adaptive geometric attributes is generated such as curvature, coherence, chaos, variance and phase Laplacian as a function of frequency. Principal component analysis (PCA) is used to produce a composite fault attribute which shows the principal orthogonal projections where the data has the largest variance. Generally, the first few principal components are sufficient to account for the large majority of the variance in the data. The composite attribute was then post-processed with a sharpening algorithm and a noise removing chaos filter. Volumetric true dip and strike were then measured on the PCA fault attribute. The PCA fault attribute shows significantly different, and geologically more plausible, three-dimensional fault distributions than conventional seismic attributes, such as curvature. Two distinct fault trends approximately 40°-50° NE-SW and 50°-60° NW-SE are observed in the Bakken Formation. Seismically derived fault orientations correlate to borehole image log data in the wells. We observed conjugate fault geometries in the seismic horizon and an apparent flip in dip direction of faults along strike. Those faults may result in widening of the faulted area and localized thinning of the rock sequence where the faults intersect, and could potentially enhance permeability along fault strike.

LINKAGES BETWEEN PETROLEUM WITHDRAWAL AND SUBSIDENCE IN GALVESTON COUNTY

KEARNS, T. J., AND G. WANG

Permanent GPS observations indicate that land subsidence has largely ceased (< -3 mm/yr) in Galveston County. Land subsidence has been steadily decreasing since the Harris Galveston Subsidence District (HGSD) began implementing groundwater withdrawal regulations in the 1970s. However, some localized subsidence has continued to occur southeast of the University of Houston (main campus) in an area that encompasses parts of the cities of Texas City, Santa Fe, Hitchcock, La Marque and Dickinson. This subsidence area has contracted from 2012-2015. In order to better evaluate linkages between land subsidence and subsurface fluid withdrawal, both groundwater levels and petroleum production was assessed. Land subsidence was based on sub-centimeter daily positions of GPS antennas (daily change in vertical displacement) from Continuously Operating Reference Stations (CORS) and Port-A-Measure Stations (PAMS) and were calculated using the Precise Point Positioning (PPP) method with Single Receiver Phase Ambiguity (SRPA) and the GIPSY-OASIS software package (V6.4). In this study only permanent GPS stations with a recording history of a least five years were used to investigate land subsidence. Measurements from 29 groundwater wells completed within the Chicot aquifer were used to determine groundwater levels below the land surface. The measurements indicate that groundwater has been above the preconsolidation level since the early 1980s. During our observation period (1993-2015) the average groundwater level was 14.3 meters below the land surface. Petroleum production was determined by evaluating 3,570 wells. Among those wells, 915 contained production data across 217 fields and 457 leases. The petroleum production includes gas (BOE), condensate (BBL) and oil (BBL) data. Observations indicate a possible correlation between petroleum withdrawal and land subsidence within the subsidence area between 2005 and 2015. Observations also suggest that there may be a period of delay between when the quantity of petroleum withdrawal substantially changes and when subsidence levels are influenced. Results from the subsidence area indicate that if groundwater in the Chicot aquifer remains above preconsolidation levels and petroleum production remains at or below current levels that the subsidence area will continue to contract and disappear as subsidence ceases entirely.

WATER OF THE CANADIAN CORDILLERA AND SLAVE CRATON LITHOSPHERIC MANTLE: AN FTIR STUDY

KILGORE, M., A. PESLIER, AND A. BRANDON

Water, or trace H incorporated in mantle mineral defects, could be a key player in the evolution of continental lithosphere because of its influence on melting and deformation of the mantle. Minerals from peridotite xenoliths are being analyzed for water by FTIR and for major elements by electron microprobe. The Alligator Lake xenoliths, representing mantle beneath the Phanerozoic belt of Western Canada, comprise lherzolites and harzburgites with contrasting trace element patterns, and are found in alkali basalts. Their orthopyroxene (opx) and clinopyroxene (cpx) contain 27-150 and 46-361 ppm wt H2O respectively. These concentrations are at the low end of the worldwide range of off-craton peridotite xenoliths. These water contents follow melting trends, and are likely not linked to metasomatism. Slave craton peridotite xenoliths, representing deeper mantle lithosphere beneath an Archean craton, ascended in kimberlites. The cpx of the Lac de Gras suite from central Slave craton have similar water contents to those of Alligator Lake but those of the opx extend to 225 ppm H2O. Olivine water contents are low (< 5 ppm H2O) at Alligator Lake which may be due to H loss during xenolith ascent, while olivines at Lac de Gras contain 30-85 ppm wt H2O. The Slave craton is lithologically layered with chemically distinct areas with depth. Preliminary data of Jericho olivine indicates that the upper spinel peridotite layer is depleted in water (<18 ppm), while deeper layers indicated extensive hydration of olivine (up to 320 ppm H2O).

CLOSE-RANGE GROUND-BASED HYPERSPECTRAL MAPPING OF A COPPER-GOLD-MOLYBDENUM PORPHYRY DEPOSIT: INSIGHTS INTO HYDROTHERMAL ALTERATION PROCESSES

KRUPNIK, D.

Approximately 45 percent of the world's copper reserves are within porphyry copper deposits. Copper porphyry mineralization is associated with certain original and alteration mineral assemblages. Identification of these minerals at outcrop scale can provide information about the different stages of alteration, which are associated with lateral and vertical zonation of a typical Copper-Gold-Molybdenum (Cu-Au-Mo) deposit. This work seeks to expand on previous studies of hyperspectral drill core analysis of this type of porphyry deposit by mapping mineralogical alteration assemblages at outcrop scale in a Cu-Au-Mo deposit in North America. A ground-based hyperspectral scanning system with sensors collecting data in the Visible Near Infrared (VNIR) and Short-Wave Infrared (SWIR) portions of the electromagnetic (EM) spectrum are utilized for close-range outcrop scanning. Data are processed and evaluated using Mixture-Tuned Matched Filtering (MTMF) and Spectral Feature Fitting (SFF) algorithms. Alteration minerals which are active in the SWIR portion of the EM spectrum are the main focus of this work. Rock samples collected from the outcrop are scanned in the laboratory setting to establish ground truth for field-based data. The objective of this ongoing study is to demonstrate the possibility of a relatively inexpensive and quick method of outcrop mapping for mining applications, allowing inaccessible cliff faces to be evaluated remotely.

THE RELATIONSHIP BETWEEN OZONE EXCEEDANCE AND THE METEOROLOGICAL EVENTS IN THE HOUSTON-GALVESTON-BRAZORIA AREA

LEI, R., S. C. WANG, Y. WANG, AND R. TALBOT

This study aims to improve the current understanding of the causes and effects of high ozone events in the HGB (Houston-Galveston-Brazoria) area. We identified ozone exceedance events and high local photochemical production (heat waves and stagnation) events across the HGB area during the ozone season (April through October) 2000-2015. The relationship between exceedance days and the meteorological event days has been characterized.

UNDERSTANDING SLAB-MANTLE INTERACTION BY 3D SEISMIC IMAGING OF REFLECTIVITY IN THE MANTLE WEDGE

LI, L., H. HU, X. LI, AND Y. ZHENG

We use seismic waves radiated by deep subduction-zone earthquakes to image possible reflectors shallower than the earthquakes. To mitigate the uncertainties of the source depth determination and velocity heterogeneities along the ray path, we first pick the energetic pP (or sP and sH; lowercase, upgoing wave; upper case, downgoing after being reflected by the surface) phase as a reference phase. pP represents a ray geometry that an upgoing P wave leaving from the source is reflected at the Earth surface and emerges at the station. Any underside reflection by a reflector above the source should produce a precursory phase to the reference phase. We use our 3D elastic Kirchhoff migration to migrate these precursory phases to image possible reflectors in the mantle wedge. To do this, we have collected 3-component broadband seismic data from IRIS generated by earthquakes (magnitude >5) occurring in the time window spanning from 2006 to 2015 recorded by global seismographs to produce 3D images of the mantle wedge. We first validate our imaging algorithm in Tonga subduction zone. We examined 530373 P-waves from567 earthquakes visually and picked 18928 high signal-to-noise traces in the imaging. In the image, discontinuities such as the Gutenberg and the '410 km' phase boundary are clearly seen. Localized reflectors due to impedance changes around 210km depth and around 330km depth are also imaged. The results agree with those in previous works. We will show results in other subduction zones, which include Java, Mariana, Japan, Kurile, and South America to systematically understand slab mantle interactions in various subduction environments.

THE METAMORPHIC P-T PATH OF THE PAMIR MUZTAGHATA DOME

LI, Y. AND A. ROBINSON

The Muztaghata gneiss dome stands on the easternmost margin of the Pamir plateau. This dome presents omphacite bearing granulites, indicating that the peak metamorphic condition is much higher than high amphibolite to granulite facies from the previous estimations. In this study, Perple_X phase diagram modeling and multiple conventional thermobarometers are applied to re-evaluate the P-T history of pelitic garnet gneiss, garnet amphibolite, and omphacite bearing mafic granulite in Muztaghata. The two pelitic garnet gneisses experienced peak metamorphic conditions of 700°C/11kbar, then retrograded to 730-770°C/7-9kbar with low degree partial melting. The omphacite bearing mafic granulite experienced peak conditions of 900-1000°C/23-25kbar with c. 1.5% partial melting, then retrograded to 850°C/14kbar and 600-700°C/9-10kbar. The chlorite and biotite-bearing garnet amphibolite only records retrograde metamorphism at 500-650°C/5-9kbar. Our results are the first documented eclogite facies metamorphism from the Pamir gneiss domes, suggesting significantly more exhumation of the Muztaghata dome than other gneiss domes in the region.

IMPROVED GEOCHEMICAL CORRELATION METHODS FOR DETERMINATION OF ORIGINS OF PETROLEUM FLUIDS

MEI, M., K. K. A. BISSADA, T. B. MALLOY, L. M.DARNELL, E. B. SZYMCYK, T. SUN, AND Z. LIU

The routine approaches for determination of origins of petroleum fluids are burdened with numerous uncertainties, ambiguities, inconsistencies and other problems that often lead to inconclusive interpretations. These complications must be analyzed carefully and the inconsistencies examined objectively. The objective of this study is to investigate the molecular and isotope geochemistry of petroleum fluids and source rocks to improve traditional correlation methods. The results involved an improved C7 hydrocarbon template for determination of fluid alterations, adjusted-diamondoid indices for correlation of thermal maturity, and a modified biomarker template for source facies interpretation. The petroleum samples were analyzed using an improved whole-oil GC-MS/MS method for simultaneous analysis of various types of molecular markers without group-type chromatographic pre-separation and multiple analytical runs of discrete fractions. This approach avoids loss of light-end components and minimizes co-elution problems. The modified methods were applied to petroleum exploration cases of southwestern Wyoming province and the Arabian Gulf.

SURFICIAL MINERALOGICAL HETEROGENEITIES AS POSSIBLE LATE DIAGENETIC INDICATORS OF MICROSEEPAGE IN GARZA, TEXAS

OKYAY, U.

The main objective of this study is to evaluate surficial mineralogical heterogeneities in the sandstone of Dockum Group as possible late diagenetic indicators of microseepage in Garza using remote sensing, geochemical, and isotope data. Laboratory-based reflectance spectroscopy analysis was performed on the collected sandstone samples providing information on the general spectral pattern of the samples and identified distinct spectral features of characteristic diagenetic minerals. Multispectral satellite data were analyzed using robust image processing methods minimizing the user bias. Complementary to the remote spectral analyses, thin section studies, major, minor, and trace element analyses, and stable carbon isotope analysis were performed. Reflectance spectroscopy, thin section studies, and geochemical analyses confirmed a reducing environment inducing the alteration and provided compositional differences reflecting the effect of reducing fluid whereas, carbon isotope analysis provided insight on the origin of the reducing fluid. Surficial mineralogical heterogeneities have been identified on the satellite imagery based on spectral properties of iron oxide and clay minerals reflecting relative abundances of these mineral groups in the satellite data. The surficial mineralogical changes, however, do not suggest zones of alteration that would fit previously described microseepage-induced alteration model and pattern. The identified areas of low iron oxide and high clay content are mostly stratabound and not restricted to extent of oil fields. In addition, high carbon isotopic composition of the altered sandstone suggested little if any proportion of oxidized hydrocarbon incorporated in the reducing fluid. Thus, despite known accumulations underground, the surficial alteration in the area may not be a direct result of microseepage.

CONSTRUCTING A HIGH RESOLUTION EVENT STRATIGRAPHY MODEL OF THE CENOMANIAN – TURONIAN OCEANIC ANOXIC EVENT 2 IN A NEOTROPICAL EPICONTINENTAL SEA

PAEZ-REYES, M., J. C. S. TAMAYO, C. JUNIUM, H. CARVAJAL-ORTIZ, AND B. MILLER

The potential usefulness of stratigraphic models for correlations at a desired spatial scale depends on the definition of consistent geochemical, paleobiological, and stratigraphic events. Usually, for intrabasinal correlations, a small number of events can provide enough resolution to achieve reliable correlations in a relatively robust stratigraphic framework. However, when rock units from a particular area need to be put in a broader context, geological correlations inevitably require the establishment of numerous tie points. As a case study, we present an event based stratigraphic model for the Cenomanian – Turonian oceanic anoxic event 2 (OAE2) in the Colombian Cretaceous Basin. This study highlights the importance of using complementary geological tools to achieve not only intrabasinal but also extrabasinal correlations. For intrabasinal correlations, our model relies on rock microfacies analysis, organic geochemistry, and stratigraphic distribution of ash layers, whereas extrabasinal correlations rely mainly on the use of stable carbon isotopes. Based on the available data, the Cenomanian-Turonian OAE2 in Colombia is characterized by: 1) the change from impure biomicrites of foraminifera to finely laminated biomicrites of foraminifera, 2) a predominance of kerogen type 1 and 2 and elevated but fluctuating values of total organic carbon, and 3) the presence of ca. 60 bentonite ash layers interbedded with the sedimentary rocks. Preliminary isotopic data show a positive δ13Corg isotopic anomaly of 7‰ and a well defined architecture of the anomaly in both sections that includes: 1) a rapid rise in the values of δ13Corg at the onset of the event, 2) a negative internal excursion in δ13Corg in the lower part of the event, 3) relatively constant δ13Corg values during the middle part of the event, and 4) a return to preexcursion δ13Corg at the end of OAE2. Future refinement of the model will incorporate other geological proxies that include trace elements chemostratigrahy, U/Pb zircon dates from ash layers, osmium isotopes, and biostratigraphy of ammonites, palynomorphs and foraminifera.

CRUSTAL STRUCTURE AND RIFT TO PASSIVE MARGIN TECTONIC EVOLUTION OF CONJUGATE VOLCANIC PASSIVE MARGINS OF THE SOUTH ATLANTIC OCEAN COMPARED TO RIFT ZONES WORLDWIDE

REUBER, K.

Volcanic passive margins (VPM) initiate during the continental rifting phase with the eruption of flood basalts derived from an underlying, active, mantle plume. Magmatism on conjugate VPM's increases in volume and intensity during continued lithospheric stretching and includes the generation of igneous belts ranging from 10-200 km in width and to 8-24 km thick. Conjugate volcanic passive margin belts form in the post-rift, early seafloor spreading phase and include seaward-dipping reflectors (SDR's) whose dips range from 0-20°. I use 27,500 line km of 40-km-record 2D seismic reflection data to investigate VPM's along the conjugate margins of the South America (Brazil and Uruguay) and West Africa (Namibia). An asymmetrical distribution of SDR's is proposed as a consequence of increased plate velocities relative to a fixed mantle position. My model integrates the addition of crustal material at a mid-oceanic spreading center but does not require simple shear to produce the observed asymmetries of the conjugate. The faster plate – South America - contains 30% less volume of SDR's (201,700 km3) compared to the slower plate – Africa (296,400 km3). I identify rifting along crustal weaknesses inherited from Paleozoic orogenic belts oriented either parallel or perpendicular to the Cretaceous rift margin. Crustal stretching factors were compiled for the South Atlantic conjugate margins and were calculated for: 1) two rift-orthogonal orogenic belts (4.3-5); 2) two suture zones and two rift-parallel orogenic belts (2.5-3.5). Obliquely-oriented orogenic belts show evidence for moderate thinning. Rift-orthogonal orogenic belts with high thinning factors resist continental rupture in the form of thinning as evidenced by 140-210+ km-wide zones of rifting. Rift-parallel orogenic belts with low stretching factors have narrow, 65-85 km-wide zones of rifting, whereas pre-existing zones of weakness are reactivated over narrow zones during the rift phase. The relationship between crustal and trend of crustal fabric from South Atlantic conjugate margins is supported by my compilation of thinning factors from 45, other rift zones worldwide.

GAS-POCKET-RESERVOIR ANALYSES UTILIZING VECTOR-BASED TO IMAGING AND EXTRACTING ROCK PROPERTIES

THONGSANG, P. AND H. HU

Pocket reservoirs a major gas production in gulf of Thailand. Due to theirs thicknesses, seismic waves when propagate through this specific reservoir type will oscillate and this phenomenon causes some difficulties in seismic migration and inversion. My study aim to tackle these obstacles by using reverse time migration (RTM) via Poynting vectors, in which improves seismic imaging and inverts prestack seismic to rock properties. I propose two methods to handle these challenges. Firstly, imaging pocket reservoirs without fluid information is the beginning to correct the reflection fidelity before conveying to seismic inversion. My work demonstrates that RTM using Poynting vectors for binning ADCIGs is better than ray-based method because obtained data are full waveforms. This specialty exhibit selective angle-stacks, which is effective to stack near and far angles separately, rather than summing all image points at one like RTM. Clearly, beneath the reservoir zones far angle-stacks can recover the missing subsurface structures, whereas near angle-stacks provide better amplitude balancing over RTM. There are processing ADCIGs workflow applied beforehand, namely, (1) high-pass filter and (2) concurrent vector-median-filter (C-VMF). The successive seismic sections necessitate flattening horizons in ADCIGs and balancing amplitudes before summing wide angle-stacks. Secondly, once obtaining pocket reservoir imaging, converting seismic to rock properties is to another objective here. Note that Poynting vectors have optional angle-stacks; hence in a complex area where near angles are distorted or attenuated, far angle-stacks can be a candidate in this circumstance. This advantage giving seismic reflections have better fidelity when compute inverting density and S-wave velocity with assisting of variable angles. I believe that this method can retrieve some covered information of rock properties, improving from initiated smooth velocity to be finer layering. This study creates innovative workflow to reduce time of building velocity migration because Poynting vectors work well in approximated velocity and on top of that C-VMF can manipulate relaxed-constraint concave events in case of incomplete flattering in ADCIGs. Consequently, migration image will end up with revealing more subsurface structures and once these reflections exposing, an opportunity of inverted data escalating.

PALEOGENE, MEGA-MASS TRANSPORT COMPLEXES IN THE DEEP-WATER FOZ DO AMAZONAS BASIN, NORTHERN BRAZIL: IMPLICATIONS FOR FUTURE HYDROCARBON EXPLORATION

TORRADO, L.

The Foz do Amazonas basin, located along the northwestern Brazilian equatorial continental margin, covers an area of about 360,000 km2. The basin is bound to the south by the Neogene Amazon Cone, to the north-west by the Amapá Platform and to the east by the Ceará Rise. The steep shelf edge of the deep-water part of the Foz do Amazonas basin has been affected during the Cenozoic by gravitational tectonics with normal faulting, folding, thrusting, and intense mass wasting processes along the shelf. Based on 21,369 km of 2D-depth-converted seismic lines and 3 exploration wells, I conducted seismic facies analysis and geomorphology on Paleogene mass transport complexes (MTCs), in order to: 1) seismically characterize gravity-induced deposits; 2) understand depositional controls on potential stratigraphic traps and seals; and 3) assess hazards for future exploration campaigns; the Paleogene section of the deep-water Foz do Amazonas basin is characterized by overpressured, heterogenic, and carbonate-rich (?) mass transport complexes of the Amapá Formation; these vast, slope-attached MTCs have wide, aerial extent (~30,000 km2), size (~600 m thick) and evacuated volume (~ 17,000 km3); the size of these pre-Amazon Cone MTCs are ten times the size of the Storegga slide in Norway, which is the largest mass-transport complex reported worldwide. Examples of these Paleogene MTC's in the Amazon fan include: 1) The Amazonas Mega-slide: a vast slide observed in seismic as moderate to high-amplitude, semi-continuous reflection packages with intense polygonal faulting; the head scarp of the Amazonas Mega-slide presents a distinctive semi-circular shape, known as a "cookie bite" formed by upper-slope collapse, and; 2) the Marajó Mega-MTC: a debris flow characterized by chaotic to contoured, low to moderate amplitude strength reflections with preservation of erosional remnants shadows and rafted blocks. Deposition of these MTCs occurred along a detachment surface of overpressured Eocene shales during a time of Oligocene to Late Miocene lowering global sea level. The casual mechanism is intense karstification from freshwater of the fluvial Travosas Formation and subsequent collapse of the Amapá carbonate platform. MTC's represent intervals of poorly preserved petroleum system elements and overpressured features considered to be drilling hazards.

INVESTIGATION OF UPSTREAM NATURAL GAS FUGITIVE LEAK DETECTION

YANG, S., R. TALBOT, AND M. B.FRISH

The U.S. is now the world's largest natural gas producer due to the expansion of horizontal drilling and hydraulic fracturing leading the increase of U.S. natural gas development. About 2% of this gas resource is wasted through leaks in the production chain. Methane (CH4) is the main constituent of nature gas. Existing CH4 monitoring devices have limitations in precisely, consistently, and cost-effectively locating and quantifying leakage rates. This project is part of the Methane Observation Networks with Innovative Technology to Obtain Reductions (MONITOR) program which aims at addressing the shortcomings of traditional methods by developing and introducing innovative technologies. The measurement system combines laser remote methane leak detector (RMLD), a small unmanned aerial vehicle as well as a real-time GPS which can provide advances in leak detection capabilities and improve the accuracy of CH4 detection. Several field tests have been done at simulated wellheads. Early data is gathered and analyzed to design prototype systems and to support the optimization of leak calculation algorithms. The noise of sensor and GPS are analyzed to clarify the influence of the measurements to the flux calculation. Up to 50% noise in the concentration measurements add less than 25% error to the flux calculation, and up to 2-meter GPS position measurements can add more than 100% error to the flux results. The measurement system has gone through several test stages using various system designs. Eventually, the system will continually and autonomously monitor gas wellheads for leakage, locate them, quantify leakage rates, and finally transmit leak information to well site operators.

AN OPTIMUM SAMPLE PREPARATION METHOD FOR MULTI-ELEMENT ANALYSIS IN CRUDE OR FUEL OILS WITH ICP-OES AND QQQ-ICP-MS BY MINERALIZATION UTILIZING A SINGLE-REACTION-CHAMBER MICROWAVE SYSTEM

YANG, W., J. F. CASEY, AND Y. GAO

A sample preparation method was developed to accurately and precisely analyze up to 57 elements in crude oils and fuel oils by ICP-OES and QQQ-ICP-MS. To eliminate spectral and polyatomic interferences caused by complex organic matrix of crude oils, we decomposed oil samples to form aqueous solutions using strong-acid digestions. Our test of many strong-acid preparation techniques included combustion followed by digestion, Parr Bomb acid digestions, and single reaction chamber (SRC) microwave assisted acid digestions. A synthetic multi-element metallo-organic standard from Conostan Oil Analysis Standards (USA) was tested thoroughly for recovery of analytes by each digestion method. No element showed recovery above 75% in our best combustion test, whereas based on 5 replicate digestions, Parr Bomb average recoveries ranged from 94% to 106% for 19 elements, and SRC microwave test average recoveries ranged from 93% to 113% for 19 elements as well. A drawback of the Parr method was a rather small sample sizes (0.1g), which placed limits on method detection limit (MDL) and method quantitation limit (MQL). Because of rapid sample throughput and the larger sample sizes (1.2g), SRC microwave digestion method was chosen to achieve better MDL and MQL on a range of elements. We then successfully tested SRC recovery (90-110%) for 57 elements in standards added to a Conostan base oil. The SRC technique was used to digest a NIST RM 8505 natural crude oil in an attempt to quantify up to 57 elements, based on 5 replicate digestions and analyses. We were able to precisely and accurately match the only recommended value referenced by NIST RM 8505 for vanadium, which is reported as 390±10 µg/g. Our result is 390±0.4 µg/g. We were able to precisely quantify 52 elements, with %RSDs of <5% for 38 elements, 5-10% for 10 elements, and 10-15.6% for 4 elements, all meeting our acceptability limits of <20% RSD. B, Nb, and W, although above MQL, were judged unacceptable because their RSDs were >31.4%, whereas Ag and Tl were below MQL, and their RSDs were >44.2% and judged unacceptable as well; although these elements have been quantified in other natural crude oils.

GEOCHEMICAL CHARACTERISTICS OF MONTEREY FORMATION, SANTA MARIA BASIN

ZHAO, B., C. BARNETTE, A. BISSADA, A. BRANDON, AND Q. FU

Stable carbon and hydrogen isotope compositions of organic compounds in sedimentary basins have been used as effective tools to understand depositional environments, source rocks, and oil generation pathways. In particular, the carbon isotope values of different groups of soluble organic compounds, including saturated, aromatic, resin, and asphaltene (SARA) components, can constrain the carbon source and depositional environment of sediments. In this study, a set of samples have been retrieved from Monterey formation (Union Leroy 51-18 well) in the Santa Maria basin. The results of carbon isotope analysis have shown that among the SARA components, the δ13C value increases with molecule complexity, i.e., from saturated hydrocarbons to resins and asphaltenes. However, aromatic hydrocarbons (-26.7‰ to -23.3‰) are always more enriched in 13C than others. The carbon isotope values of bitumen are in the range of -24.9 to -22.6‰. Within two different lithofacies, phosphatic carbonate and siliceous shale facies, which are identified by previous studies, the siliceous shale has higher d13C values than phosphatic carbonate facies. This may be due to the different depositional environment that affects carbon isotope values. The phosphatic carbonate deposited under higher sea-level conditions than siliceous shale facies. There is no major change in δ13C values of SARA components within these two lithofacies. Further studies on stable hydrogen isotopes of n-alkanes along with the analysis of kerogen would help evaluate the hydrogen source and paleo-environment change during diagenesis.

ELASTIC PROPERTIES OF SALT

ZONG, J., R. R. STEWART, AND N. DYAUR

Rock salt is a special type of sedimentary rock that has played a large role throughout tec- tonic and economic history. Salt's unique physical properties (ductility, low density, flowability, and impermeability) can be critical factors in hydrocarbon traps and underground storage. However, seismic imaging and interpretation of regions with salt structures can be challenging due to salt's complex geometry and large impedance contrast with surrounding rocks. We are thus motivated to investigate the elastic properties of rock salt. To connect salt's properties and state to elastic values, we use ultrasonic laboratory measurements and well logs. In the lab, we have analyzed the effects of composition, crystalline structure, pressure, and temperature on the elastic behavior of a variety of rock salt samples. The samples include pure halite (>95 wt.%) from the Gulf of Mexico (GoM) area, argillaceous rock salt from the Zipaquiŕa Mine, Colombia, and crystalline salt from the Goderich Mine, Canada. Current measurements suggest that the GoM salt cores behaved isotropically in general. The Zipaquiŕa salt samples showed velocity and density variations on account of their heterogeneous composition. The Goderich halite crystals displayed distinct cubic anisotropy. Measurements on the GoM samples at varying confining pressures and temperatures indicated that increasing pressure elevated velocity while increasing temperature decreased velocity. From the analysis of 145 log suites from boreholes drilled through salt in the northern GoM, we found that within the salt formations, the P-wave velocities increase slightly with depth (around 5 m/s per km). The S-wave velocities from three wells range from 2280 to 2580 m/s. The bulk densities from all the wells cluster at 2160 ± 30 kg/m3. These lab and log measurements provide new values for salt's elastic properties which can assist in velocity model building, synthetic seismogram generation, and the understanding of halite's rock physics.